Drexel University

Annual Progress Report: 2009 Formula Grant

Reporting Period

January 1, 2010 – June 30, 2010

Formula Grant Overview

The Drexel University received $1,431,165 in formula funds for the grant award period January 1, 2010 through December 31, 2010. Accomplishments for the reporting period are described below.

Research Project 1: Project Title and Purpose

Effect of Antiretroviral Therapy on Surrogate Markers of Cardiovascular Disease and Inflammation in HIV-infected Patients - Numerous studies have demonstrated that HIV infected patients are at an increased risk of developing cardiovascular disease (CVD) and myocardial infarction (MI). There is evidence to suggest that HIV infected patients have unique risk factors related to their infection and its treatment that interact with traditional cardiac risk factors to put them at increased risk of CVD. The purpose of this study is to prospectively evaluate measures of endothelial function and subclinical atherosclerosis as well as markers of inflammation in HIV patients in order to elucidate the nature of HIV specific risk factors for cardiovascular disease. This knowledge will allow more effective risk stratification and treatment in this population which is disproportionally affected by cardiovascular disease.

Anticipated Duration of Project

1/1/2010 - 12/31/2010

Project Overview

We will conduct a prospective cohort study examining the affect of initiating Anti-retroviral therapy (ART) on structural, immunologic, and functional markers of atherosclerosis. We hypothesize that although some components of ART may carry increased risk of CVD, the net effect of viral suppression will be decreased inflammation with resultant decreased atherogenesis and improved endothelial function. Our study will address the following specific aims:

Specific Aim 1: To determine if HIV infection is associated with increased inflammation decreased endothelial function, and increased risk for atherosclerosis.
Specific Aim 2: To determine if initiation of ART in HIV infected adults is associated with improvement of markers of inflammation, endothelial function and atherosclerosis.
Specific Aim 3: To asses for correlation between changes in immune activation and changes in markers of inflammation and subclinical atherosclerosis.

We will accomplish these aims by conducting a prospective observational cohort study focusing on 3 groups: HIV infected subjects who initiate ART, HIV infected subjects who do not initiate ART, and HIV negative subjects with the following specific objectives: 1) To compare mean change at one year in carotid artery intima-media thickness (IMT) between the three study groups. 2) To compare changes in inflammatory markers, brachial artery Flow Mediated Dilation (FMD), cardiac ejection fraction and pulmonary artery pressure at one year between the three study groups. 3) To asses for correlation between changes in serum markers of inflammation, status of HIV disease (as measured by CD4 and viral load), endothelial activation, physiologic surrogates of CVD such as IMT and FMD and cardiac function.

Principal Investigator

Christopher J. Bruno, MD
Assistant Professor of Medicine
Drexel University College of Medicine
245 N. 15th Street
Mail Stop 461
Philadelphia, PA 19102

Other Participating Researchers

Jeffrey Jacobson, MD, Howard Eisen, MD, Andrew Kohut, MD, Michele Kutzler, PhD – employed by Drexel University College of Medicine

Expected Research Outcomes and Benefits

As HIV-infected patients live longer, the recognition and treatment of other chronic illnesses has taken on increased significance in this population. Cardiovascular disease (CVD) is of particular importance since several large cohort studies have demonstrated an increased prevalence of CVD, and a higher risk for myocardial infarction (MI) in HIV-infected patients in the ART era.

This study will collect preliminary data that will allow us to begin to correlate observations from the clinical realm with changes at the molecular level to better understand the mechanisms of atherosclerotic disease in HIV infected patients. Measurement of circulating markers of immune and endothelial activation will provide an insight into the pathophysiology of CVD at the molecular level. Structural and functional measurements of atherosclerosis will provide a macroscopic correlate. We expect that through this approach we will gain a better understanding of the pathophysiology of this process with the long term goal of establishing biomarkers of CVD in HIV infected patients that can be used in combination with clinical data to predict and monitor CVD in HIV patients in clinical care.

Summary of Research Completed

During this reporting period it became clear that results from one of the study procedures, the brachial artery flow-mediated dilation (FMD) were not reliably reproducible using the equipment and personnel available. Enrollment was put on hold while the protocol was revised to remove

this procedure. For this reason we did not enroll any subjects and have not expended any of the grant funds. We believe that we can still assess endothelial function using serum markers such as Intercellular Adhesion Molceule-1 (ICAM-1) and Vascular cell adhesion Molecule-1(VCAM-1) and correlate this with the structural markers of atherosclerosis (carotid artery intima-media thickness) and markers of immune activation and HIV status. We anticipate that we will be able to complete the enrollment as originally planned.

Research Project 2: Project Title and Purpose

Modulation of Capsid Stability as an Antiviral Strategy - The project purpose is to identify anti-HIV compounds that work by antagonizing the functions of the viral capsid protein.

Anticipated Duration of Project

1/1/2010 - 12/31/2010

Project Overview

The HIV-1 capsid (CA) is an essential viral protein that performs two major roles in the life cycle of HIV-1: one structural, in which it forms a protein shell that shields both the viral genome and the replicative enzymes of HIV-1, and the other regulatory, in which the precise temporal disassembly of this shell coordinates post-entry events such as reverse transcription. The CA protein is composed of two domains: the C-terminal domain (CTD) and the N-terminal domain (NTD). Both of these domains make critical inter- and intradomain interactions that are critical for the formation of the capsid shell. Recently, the atomic structure of the hexameric building block of the HIV-1 capsid shell has been determined. This structure offers new insights into the molecular details of the hexameric assembly of CA, in particular revealing features of the NTD-NTD interface that may be exploited therapeutically.

The NTD of the capsid protein is the structural anchor for the formation of the hexameric lattice by which the HIV-1 capsid assembles. The stability of this hexameric lattice, which is also conferred by the NTD, regulates the precise temporal series of replicative events after fusion; capsids that are too stable or too unstable do not enter into reverse transcription correctly. Therefore, in theory, any compound that disrupts the normal interactions of the capsid—whether by inhibiting assembly, accelerating disassembly, or artificially stabilizing the core—should attenuate or even kill the virus. The essential roles played by capsid within the HIV-1 life cycle, coupled with the existence of known compounds with the ability to disrupt CA-CA interactions, make the capsid's hexamerization interface a new, attractive therapeutic target.

We therefore propose to identify and characterize the properties of novel small molecules that bind at the NTD-NTD interface. This will be achieved using the newly available structure of the hexameric HIV-1 capsid lattice in conjunction with the novel hybrid structure–based (HSB) in silico screening protocol. Small-molecule "hexamerization antagonists or agonists" identified by this process would represent a new class of capsid inhibitor, targeted at a highly conserved oligomerization surface and possessing a novel mechanism of action. A cross-disciplinary approach comprised of computational, virologic, chemical, and biochemical assays will then be

employed to validate, understand, and augment such inhibitors. We believe that this strategy will successfully identify pharmacologically useful reagents that can be used to gain insight into the biological functions of HIV-1 CA protein, such as uncoating and assembly. In addition, small molecules identified from this study hold promise as lead compounds for a new class of antiviral agent.

Principal Investigator

Simon Cocklin, PhD
Research Assistant Professor
Drexel University College of Medicine
Room 10308-312
Department of Biochemistry & Molecular Biology
245 North 15th Street
Philadelphia, PA 19102

Other Participating Researchers

Sandhya Kortagere, PhD - employed by Drexel University College of Medicine
Joseph G. Sodroski, MD - employed by Dana-Farber/Harvard Cancer Center
Wesley Sundquist - employed by University of Utah
Amos B. Smith, III - employed by University of Pennsylvania

Expected Research Outcomes and Benefits

Acquired immune deficiency syndrome (AIDS), caused by the human immunodeficiency virus (HIV-1), is a global epidemic that comprises one of the world's major health problems. Currently, over 40 million people are infected with HIV-1, leading to 3 million deaths from AIDS or AIDS-related causes every year. Despite recent progress in anti-HIV therapy, drug toxicity and the emergence of drug-resistant isolates during long-term treatment of HIV-infected patients necessitate the search for new targets that can be used to develop novel antiviral agents. It is very unlikely that any single inhibitor will be the sole solution to these problems. The more stages of the viral life cycle that can be antagonized, however, the more likely it is that the virus would be forced to mutate at the expense of its fitness, and the less likely that enough viral replication would occur to generate escape mutants. Given the essential roles, both structural and regulatory, of capsid within the HIV-1 life cycle, and the existence of compounds with the ability to disrupt CA-CA interactions, the capsid comprises a tractable therapeutic target. In this project we will identify, characterize, and augment novel small molecules designed to bind the capsid and antagonize its function. These "capsid hexamerization antagonists or agonists" would represent a new class of small-molecule capsid inhibitors, targeted at a highly conserved oligomerization surface and possessing a novel mechanism of action. We believe these data will not only provide new reagents for the dissection of the basic biology of HIV-1 replication and pathogenesis, but will also lay the foundation for a major new initiative in HIV-1 drug discovery.

Summary of Research Completed

Computational screening and design of small-molecule inhibitors against the NTD-NTD hexamerization interface using the hybrid structure–based (HSB) method. The capsid of the HIV-1 virus has a distinct geometry of a fullerene cone consisting of nearly 250 hexamers and 12 pentamers of the viral CA protein. Mutagenesis studies within the NTD of CA have shown that the hexamer interface is very sensitive to genetic perturbation; single point mutations can lead to a number of altered CA proteins, each of which is damaging to the virus that harbors them. Targeting protein-protein interactions for a therapeutic purpose is an attractive idea that has proved to be extremely challenging in practice using standard methods of computational screening. The HSB method utilizes the information in such "hotspots" to inform the screening procedure and has been successfully applied to design highly selective small-molecule inhibitors. We have used the HSB method to design small-molecule inhibitors targeted to the NTD-NTD hexameric interface of HIV-1 CA. These studies were performed in collaboration with Dr. Sandhya Kortagere (Department of Microbiology and Immunology).

The HSB method combines the best elements of both of these virtual screening strategies: using ligand-based methods to build enriched libraries of small molecules, and then employing a combined receptor–ligand pharmacophore to screen molecules from the enriched library and to further dock the molecules to their receptor.

Screening of a novel enriched database of small molecules using the HSB method and the structure of the HIV-1 CA protein. The first phase in the HSB method is the development of a comprehensive electronic database of commercially available small molecules. This database was generated using a subset of the Zinc database that consists of compounds from commercial vendors such as Asinex (Moscow, Russia), Maybridge (Trevillett, North Cornwall, UK), Bionet (Camelford, Cornwall, UK), Cerep (Paris, France), AMRI (Albany, NY), and TimTec (Newark, DE) along with other compounds from natural sources, ligands from the Protein Data Bank (PDB), and FDA-approved drugs. The entire database is comprised of nearly 3 million compounds. All of the commercially available compounds were acquired as sdf formatted files, converted into the Mol2 format, and energy minimized in SYBYL (Tripos, St. Louis, MO). All of the molecules in the database were filtered for redundancy and renamed according to their corresponding vendor listing.

The next phase of the HSB method is the generation of the combined ligand–protein pharmacophore (also called the hybrid pharmacophore). This phase is the key to the entire method and customizing the pharmacophore to capture the essential features of interactions occurring at the hexamerization interface of the CA_{NTD} is extremely important. A model of the CA-CA complex was prepared from PDB entry 3H4E by adding hydrogen atoms and refining the structure using energy minimization combined with a 1-ns-long molecular dynamics simulation. All simulations were performed using Amber (version 9.0), with Amber charges. The combined pharmacophore was then designed centered around those residues responsible for the stability of the interface. Site-directed mutagenesis studies have shown that residues A42 and M39 when mutated prevent capsid assembly. These two residues along with L20 from the neighboring monomer form the hydrophobic core of the hotspot, while R173 forms a critical interdomain hydrogen bond with N57 and V59. A four-point pharmacophore consisting of three

hydrophobic and one hydrogen bond donor-acceptor feature was designed using these interactions as input. The enriched database described above was then screened against this pharmacophore and first filtered according to Lipinski's "rule of five" to identify "drug-like" molecules. A second regression-based blood–brain barrier (BBB) penetration model was also applied to filter out compounds for BBB penetration. We obtained 900 hits from this pharmacophore-based screening and filtering. From these 900, we choose 300 hits for docking and scoring to the structure of a monomer isolated from the hexameric CA structure. The GOLD program (Genetic Optimisation for Ligand Docking), in "library screening mode," was employed for preliminary docking and scoring. The docking area was restricted by a sphere of 8 Å and encompassed residues from the interface region such as P38, T58, A42, M39, and L20. Given the nondeterministic nature of genetic algorithms, 50 independent docking runs were performed for each ligand. The full set of docked structures was then energy minimized using the molecular modeling package SYBYL. The docked receptor–ligand complexes were then scored using a customizable knowledge-based scoring function that is based on the nature of the interaction of every atom within the NTD-NTD docking pharmacophore. A consensus scoring scheme that involves GoldScore, ChemScore, contact score, and a shape-weighted scoring scheme was then used to rank the compounds. The best ranking complexes were visually inspected to include compounds that not only interacted with the specified residues but also had extended volume to maximize the inhibition of the NTD-NTD interface. We have thus far purchased 20 compounds from various vendors that are predicted to bind to the CA NTD-NTD interface and possess antiviral activity.

In vitro validation of the antiviral activity of the HSB-identified compounds. Although there are HIV-1 CA in vitro assembly assays that provide a facile means of testing the anti-assembly properties of candidate compounds, the gold standard remains the direct demonstration of antiviral activity. Only in this context can the effect of the compounds on the functional oligomeric HIV-1 CA/Gag be unambiguously assessed. Therefore, as a first-level screen we have monitored the potential antiviral effects of the first 20 small molecules identified from the HSB screen using a single-round infection assay. These experiments were performed in collaboration with Dr. Joseph Sodroski (Dana-Farber/Harvard Cancer Center). Infection assays of this sort have been performed in the Sodroski laboratory for more than a decade.

Single-round infection assay. We have used a single-round infection assay in order to determine whether the compounds affect early events (such as uncoating) or late events (such as assembly) or both. Details of the single-round infection assay have been published in detail elsewhere and the method has been routinely used in the Sodroski laboratory for studies of inhibitors of HIV-1 replication. Effects on assembly are identified by incubating the viral producer cells in the presence of the compound. Virus is then purified from the supernatants of the producer cells and used to infect the target cells. Aberrant assembly is manifested as a decrease in infectivity within the target cells. Similarly, uncoating effects are determined by producing virus in the absence of compound, then infecting target cells in the presence of compounds. Using this strategy, we have identified to date three novel compounds (CK026, CK422, and CK207) that inhibit either early events (pre-integration) or late events (post-integration) in HIV-1 replication (Table 1). Moreover, these compounds do not display any toxicity on either the producer or target cells up to a concentration of 100 μM as judged by a lactate dehydrogenase release assay.

Antiviral spectrum of compounds CK422 and CK026. To determine the spectrum of antiviral activity of compounds CK026 (early-stage inhibitor) and CK422 (late-stage inhibitor), we evaluated these compounds in cytoprotection effect (CPE) assays against a panel of viruses from different classes. The CPE assay uses Vero cells in conjunction with the particular virus strain. Virus and cells are mixed in the presence of test compound and incubated for 5 days. The virus is pre-titered such that control wells exhibit 85 to 95% loss of cell viability due to virus replication. Therefore, antiviral effect or cytoprotection is observed when compounds prevent virus replication. Each assay plate contains cell control wells (cells only), virus control wells (cells plus virus), compound toxicity control wells (cells plus compound only), compound colorimetric control wells (compound only), as well as experimental wells (compound plus cells plus virus). Cytoprotection and compound cytotoxicity are assessed by 3-(4,5-dimethylthiazol-2-yl)-5-(3-carboxymethoxyphenyl)-2-(4-sulfophenyl)-2H-tetrazolium (MTS; CellTiter96 Reagent; Promega, Madison, WI) dye reduction. The percent reduction in viral CPE is determined and reported; IC_{50} (concentration inhibiting virus replication by 50%), TC_{50} (concentration resulting in 50% cell death), and a calculated TI (therapeutic index = TC_{50}/IC_{50}) are provided along with a graphical representation of the antiviral activity and compound cytotoxicity when compounds are tested in dose-response. We therefore used the CPE assay to determine the spectrum of antiviral activity of compounds CK422 and CK026 against herpes simplex virus (HSV)-1 (dsDNA), influenza H1N1 (-ssRNA), vaccinia (dsDNA), and Chikungunya (+ssRNA) viruses. These results are shown in Table 1. Neither compound inhibited any of these viruses up to the maximum concentration tested (100 μM).

Cloning and expression of CA and CA-NC protein

To facilitate the biochemical/biophysical aspects of this project, we have designed and created expression constructs to drive the overproduction of two versions of the HIV-1_{NL4-3} capsid protein. Both versions of the capsid were codon-optimized for bacterial expression and synthesized by Genscript prior to subcloning into the expression vector pET11a. The two expression vectors, pET11a-CA-H_6 and pET11a-CA-NC-H_6, drive the overproduction of a C-terminally His-tagged CA protein and C-terminally His-tagged CA-nucleocapsid (NC) fusion protein, respectively. Figure 1 shows the expression of these proteins in Escherichia coli BL21(DE3) codon$^+$ RIPL cells (Stratagene, La Jolla, CA).

Chemical synthesis of analogues and fragments of CK026: towards defining the active pharmacophore

Compound CK026 was the first compound that we identified using the aforementioned strategy. This compound is larger than typical drug candidates and has suboptimal pharmacokinetic properties. Therefore, we have started to synthesize compounds designed to improve these properties and also to define the active pharmacophore. Details of two compounds that we have synthesized during the reporting period are given below. These compounds are currently undergoing antiviral testing in the single-round infection assay.

Synthesis of 4-(4,5-diphenyl-1H-imidazol-2-yl)benzoic acid (I-XW-053)

A mixture of benzil (400 mg, 1.9 mmol), 4-carboxybenzaldehyde (285.6 mg, 1.9 mmol), and

ammonium acetate (2.2 g, 28.5 mmol) in acetic acid (19 mL) was refluxed for 4 h. The resulting mixture was then cooled to room temperature and poured into ice/water. The solid was collected by filtration and purified by column chromatography (3:2, ethyl acetate/hexanes) to yield the product as a white solid (395.3 mg, 61%).

Synthesis of methyl 4-[5-[8-[2-(4-methoxycarbonylphenyl)-4-phenyl-1H-imidazol-5-yl]dibenzofuran-2-yl]-4-phenyl-1H-imidazol-2-yl]benzoate (DMJ-I-073)

To a solution of diacid 1 (10 mg, 14 mmol) in methanol/methylene chloride (1 μL, 1:1), approximately 50 μL of a 1.0-M solution of trimethylsilyldiazomethane was added at room temperature until the solution became yellow and gas was no longer evolved. The reaction was then stirred for an additional 10 min. Argon was then bubbled through the reaction mixture, and the solution was diluted with additional methylene chloride. The reaction was quenched with sat. $NaHCO_3$. The product was extracted from the aqueous layer with methylene chloride (2 × 2 mL). The combined extracts were dried with Na_2SO_4, concentrated and purified by preparative thin-layer chromatography using 1:1 hexane/ethyl acetate. 8.6 mg of DMJ-I-073 (85%).

Compound	Virus strain	High-test/ units	IC_{50} (µM)	TC_{50} (µM)	Antiviral index
CK422 Late-stage inhibitor	NL4-3	100 µM	30	> 100	> 3.34
	HSV-1		> 100		NA
	H1N1		> 100		NA
	Vaccinia		> 100		NA
	Chikungunya		> 100		NA
CK026 Early-stage inhibitor	NL4-3	100 µM	33.3	> 100	> 3.0
	HSV-1		> 100		NA
	H1N1		> 100		NA
	Vaccinia		> 100		NA
	Chikungunya		> 100		NA
CK207 Early-stage inhibitor	NL4-3	100 µM	30	> 100	> 3.34
	HSV-1		> 100		NA
	H1N1		> 100		NA
	Vaccinia		> 100		NA
	Chikungunya		> 100		NA

Table 1. Antiviral spectrum of the capsid (CA)-targeted compounds. H1N1 = influenza strain A/PR/8/34 (H1N1); HSV-1 = herpes simplex virus 1; IC_{50} = concentration inhibiting virus replication by 50%; NL4-3 = HIV-1 subtype B; TC_{50} = concentration resulting in 50% cell death.

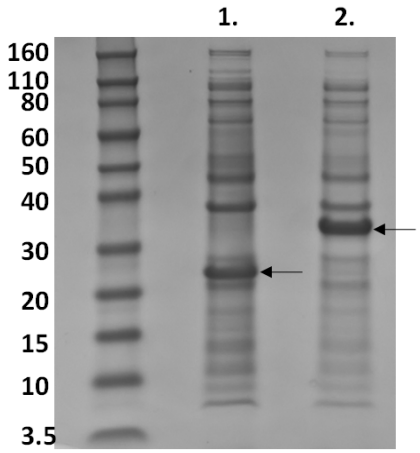

Figure 1: Sodium dodecyl sulfate–polyacrylamide gel electrophoresis (SDS-PAGE) analysis of the bacterial expression of HIV-1_{NL4-3} capsid (CA) and capsid-nucleocapsid (CA-NC) proteins. *Lane 1* = Novex Sharp Pre-stained Protein Standards (Invitrogen, Carlsbad, CA) (molecular weights in kDa). *Lane 2* = Whole cell lysate containing CA-H_6. *Lane* 3 = Whole cell lysate containing CA-NC-H_6 protein.

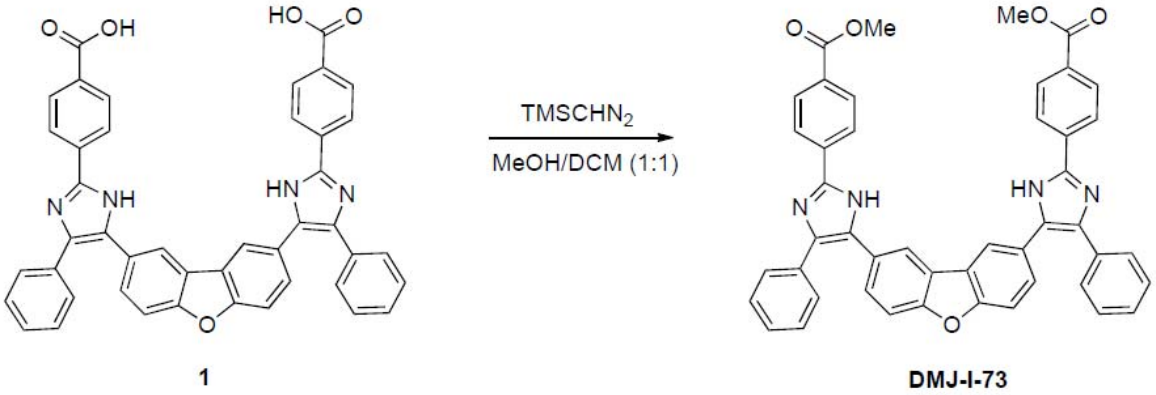

Figure 2: Chemical scheme for synthesizing DMJ-I-073.

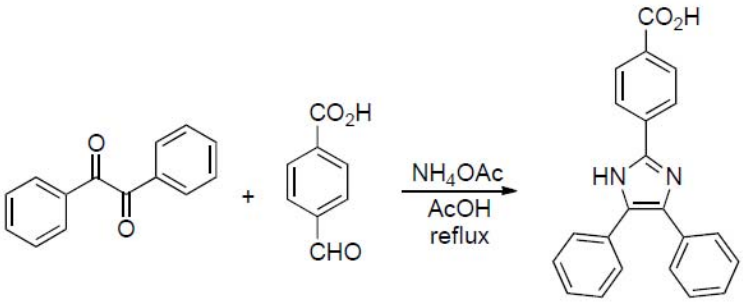

Figure 3: Chemical scheme for synthesizing I-XW-053.

Research Project 3: Project Title and Purpose

sPLA2 Inhibition Therapy for Epilepsy - This project will test the efficacy of new secreted phospholipase A2 (sPLA2) inhibitors as therapy for both the excitability disturbances and inflammatory consequences of epilepsy. These inhibitors, called CHECs, consist of 7mer and 9mer peptides with demonstrated systemic efficacy in traumatic and autoimmune disease models. They are part of a portfolio of intellectual property (composition of matter, applications, diagnostic) held by Drexel University. The goal of this application is to expedite the clinical development of these peptides by expanding potential clinical applications. These compounds are especially suited for commercial development since it has been unequivocally demonstrated that they are active when taken by mouth. The present experiments are proof-of concept studies for treatment of epilepsy, where the inflammatory consequences of the disease have been largely overlooked. Interestingly, there is also evidence, including our own preliminary studies, that excitability changes during epilepsy are closely related to inflammation, raising the possibility that the CHEC peptides represent a unique monotherapy for this disease.

Anticipated Duration of Project

1/1/2010 - 12/31/2010

Project Overview

SPECIFIC AIM 1 - Inflammation, sPLA2 inhibition and seizure control.
We will screen two systemically active peptide inhibitors of sPLA2 enzymes CHEC-7 and CHEC-9 in a kainic acid seizure model applied to early postnatal and young adult rats. A wealth of data exists that demonstrates the anti-inflammatory and survival promoting activity of these compounds, and preliminarily, their influence of excitability and synaptic functions. We will now apply these peptides to the KA model to explore both contribution and consequences of sPLA2 enzyme activity in seizure disorders. We will measure the following in P13-16 and P35-40 KA models:
a. Motor seizure activity, including potential critical periods for effective sPLA2 inhibition.
b. The time course of changes in enzyme activity, lipid products and substrates (many of the latter are potent inflammatory mediators) using assays specific for sPLA2s, 2D TLC, and mass spectroscopy. These measurements include systemic activity (plasma, urine), and the activity found in the soluble and synaptosomal fractions of cerebral cortex (including hippocampus).

SPECIFIC AIM 2. Inflammatory correlates of childhood and adolescent/young adult epilepsy.
It is our hypothesis that the period of sPLA2 elevation (relative to stable patients) represents the period of maximum vulnerability to seizure-induced inflammatory destruction of central nervous system (CNS) tissue, presumably instigated by inflammatory mediators and the cellular participants in the immune response. We therefore will measure plasma and urinary sPLA2 activity and levels of selected phospholipids in young epileptic patients and compare to seizure history. The relationship of systemic inflammation to other epidemiological and clinical parameters such as age, duration of epilepsy, type of epilepsy and medication will also be determined.

Principal Investigator

Timothy Cunningham, PhD
Professor
Drexel University College of Medicine
2900 Queen Lane
Philadelphia, PA 19129

Other Participating Researchers

Agustin Legido, MD, PhD, MBA, Ignacio Valencia, MD, Divya Subramanian-Khurana, MD – employed by Drexel University College of Medicine

Expected Research Outcomes and Benefits

These experiments are proof-of concept studies for treatment of epilepsy, where the inflammatory consequences of the disease have been largely overlooked. Interestingly, there is also evidence, including our own preliminary studies, that excitability changes during epilepsy are closely related to inflammation, raising the possibility that the CHEC peptides, that are the subject of this research, represent a unique monotherapy for this disease.

Seizures in humans produce high levels of sPLA2 making these enzymes a worthwhile therapeutic target for controlling hyperexcitability and subsequent inflammatory pathology. The CHEC peptides, which are sPLA2 inhibitors, are ideally suited for this therapy, since they are effective orally and operate on an "as needed" basis.

Summary of Research Completed

The aim our study was to test the efficacy of novel orally active secreted phospholipase A2 (sPLA2) inhibitors as monotherapy for the excitability disturbances, inflammation, and neuron death that characterize seizure disorders. Our experiments demonstrate that sPLA2 inhibitors (called CHECs) inhibit kainic acid-induced seizures and abnormal firing of hippocampal neurons. The results show clearly that CHEC peptides protect neurons that would usually degenerate following seizures. We also proposed to test the ongoing sPLA2 activity in the plasma and urine of children and young adult epilepsy patients, compared to suitable controls, to test for ongoing inflammatory activity in relation to timing and frequency of seizures. This aspect of the study has just begun. Publication of our interim results is in preparation:

Cunningham, TJ, Yao, L, Chen, S, Waterhouse, BE, and Starr, MA, *Inhibition of secreted phospholipase A2 activity inhibits Kainic acid-induced status epilepticus, neuron death and microglial activation in CA1 of hippocampus*, in preparation 2010.

Electrophysiological Studies:

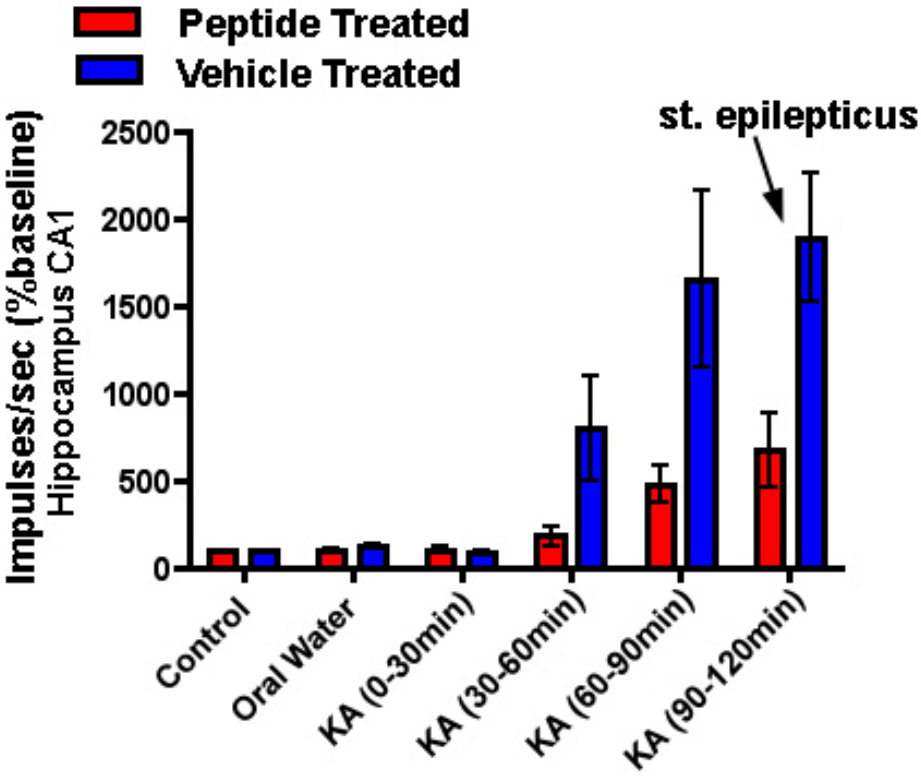

Figure. 1. Multiunit activity in the hippocampus of awake, freely moving kainic acid (KA)-treated rats with and without pretreatment with CHEC-9 or vehicle. The rats were implanted with a multichannel electrode bundle one week earlier. Baseline activity (mean firing rate, expressed in Hz) was collected during a 30min control period, followed by oral CHEC-9 (1mg/kg) or Vehicle for 40 min prior to IP kainic acid (10mg/kg). The response to the eleptogen is robust. CHEC-9 pre-treatment (n=3) significantly attenuates the kainic acid-induced increase in neuronal and seizure activities. (Vehicle treated rats (n=3) reached status epilepticus after ~1 hr.; peptide treated rats showed no obvious symptoms. See also Table 1.

Behavioral Studies:

Table 1- CHEC-9 (C9) and Vehicle (V) pre-treatment of KA-induced seizures. The behavioral results from 14 rats demonstrate that the CHEC-9 peptide inhibits kainic acid-induced status epilepticus, including via oral delivery. ** Severity is graded by a classical scale (1): 1, hypoactivity, mouth and facial automatism; 2, head nodding and mastication; 3, forelimb clonus without rearing; 4, bilateral forelimb clonus and rearing, 5, rearing and loss of posture. We define *Status epilepticus* (Stat EP) as stages 3-5 appearing continuously for 30 min. [s.c. –subcutaneous; po-oral]

Gender	C9 Dose mg/kg route	KA mg/kg ip	Max Seizure Stage**
F	V sc	5	Stat Ep
F	V po	10	Stat Ep
F	V po	10	4
M	V po	5	Stat Ep
M	V sc	6	Died
M	V sc	5	1
M	V po	10	Stat Ep
M	0.5 sc	6	2
M	1.0 po	10	1
M	1.0 po	5	1
F	1.0 po	10	3
F	0.5 sc	5	1
M	0.5 sc	5	1
F	1.0 po	10	1

Histological/Immuncytochemical Studies:

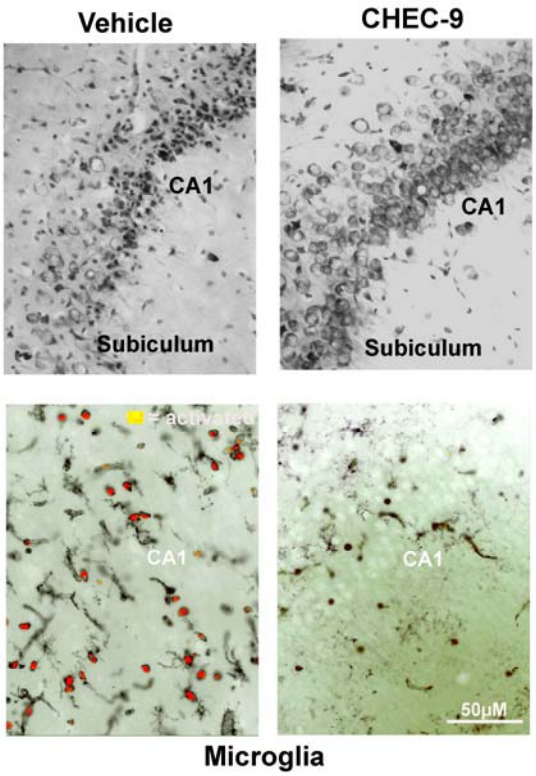

Figure 2. Inhibition of seizure activity by CHEC-9 prevents microglia activation (inflammation) and neuron death in CA1 of hippocampus. The border between CA1 and the subiculum is shown in horizontal sections. Top: Cresyl violet-stained sections showing pyramidal cells 24hrs. after kainic acid-induced status epilepticus (SE). In the vehicle treated rats the cells were degenerated. CHEC-9 inhibits SE and preserves the cells. Bottom: Adjacent double-stained with lectin IB4 (all microglia, black) and ED- (activated microglia, red). The number and activation of microglia is inhibited by CHEC-9 consistent with the neuron rescue shown above.

Research Project 4: Project Title and Purpose

Role of Septins in Growth Cone Guidance - This project will investigate the roles of three members of the septin family of GTPase (septin 2,6,7) in the guidance of growth cones by extracellular signaling molecules. The correct guidance of axons is crucial to nervous system development and regeneration following injury. The project will determine if septins are involved in growth cone guidance and the extension of axons, and thus whether they may be targets for therapeutics aimed at promoting or regulating axon extension and regeneration.

Anticipated Duration of Project

1/1/2010 - 12/31/2010

Project Overview

The broad objective of the project is to determine if septin 6 and 7 are involved in growth cone guidance using in vitro model systems and in vivo analysis of growth cone guidance. The project has two main Aims: (1) Analysis of the spatiotemporal dynamics of septins during guidance, and (2) Elucidation of the functions of septin 6 and 7 in axon extension and guidance.

Principal Investigator

Gianluca Gallo, PhD
Associate Professor
Drexel University College of Medicine
2900 Queen Lane
Philadelphia PA 19129

Other Participating Researchers

Elias Spiliotis, PhD – employed by Drexel University

Expected Research Outcomes and Benefits

The extension and guidance of axons is a fundamental aspect of the regeneration of neuronal connections following injury. A comprehensive understanding of the mechanisms of extension and guidance will provide a platform for the design of therapeutic interventions aimed at promoting regeneration or the targeting of axons following injury. This project will determine whether septin family members may be targeted to promote the extension and/or guidance of axons.

Summary of Research Completed

The main hypothesis of this proposal is that the actin and microtubule cytoskeleton is regulated by SEPT6 and SEPT7 during axon extension and growth cone guidance. Based on our preliminary data, we postulate that SEPT6 and/or 7 is required for the stabilization of actin and

filopodia during the initial phase of grown cone turning, while SEPT7 might be involved in the guidance of microtubules once polarity in the movement of the growth cone has been established.

Support from this award has allowed us to (A) generate additional in vitro data, (B) establish and develop in ovo electroporation for in vivo functional analysis, and (C) submit an National Institute of Health (NIH) R01 seeking extramural support for the project. Progress toward each of these points is outlined in the following text.

(A) In vitro studies

(Figure 1) We have extended our initial immunocytochemical analysis of septins in growth cones to cover SEPT6, SEPT7 and SEPT2. All three septins are found in embryonic sensory neuron growth cones and exhibit differential distributions. SEPT6 is found throughout filopodial shafts and within the growth cone peripheral and central domains, while SEPT7 localizes to the base of filopodia, and SEPT2 is also found throughout the growth cone.

(Figure 2A-C) We have also determined the effects of inhibiting the turnover of septins (presumably all septins) using a pharmacological tool (FCF) on the morphology of growth cones cultured in the continued presence of NGF and find that this manipulation of septins results in decreased growth cone lamellipodial formation but increase numbers of filopodia. These data provide proof of concept that septins are involved in the regulation of growth cone protrusive activity.

(Figure 3) NGF promotes the spreading of growth cone lamellipodia in sensory neurons. By culturing sensory neurons in the absence of NGF we have determined that FCF treatment inhibits the increase in lamellipodial area induced by NGF but has no effect on the area of growth cone in the absence of NGF. These data provide proof of concept that septins are involved in the regulation of growth cone lamellipodia by NGF.

(Figure 2D,E) We have determined that overexpression of SEPT2 in neurons cultured in NGF results in decreased growth cone area and filopodial numbers.

(Figure 4) We have generated a SEPT6 mutant construct (G78T) that unlike wild type SEPT6 is predicted to exhibit active GTPase activity. Expression of G78T-SEPT6 increased growth cone area, while expression of wild type SEPT6 or SEPT7 had no effects. These data suggest that promotion of SEPT6 GTPase activity can affect growth cone dynamics and pave the way for continued investigation of the role of SEPT6 in growth cone motility.

(Figure 5) We found a correlation between SEPT7 distribution and microtubule localization in growth cones. Briefly, asymmetric accumulations of microtubules in growth cones correlate with increased levels of SEPT7 (Fig 5A, B). Analysis of the targeting of microtubules to axonal filopodia revealed that overexpression of SEPT7 but not SEPT6 promotes the targeting of microtubules into filopodia (Fig 5C). Collectively these data indicate that SEPT7 may be involved in the targeting of microtubules to actin based protrusions during growth cone advance/guidance and also during axon branch formation, which are initiated by the formation of

axonal filopodia and mature through the targeting of microtubules into the filopodia. Indeed, we find that overexpression of SEPT7 also promotes axon branching (data not shown).

We have developed tools for vector-driven expression of shRNA toward SEPT6 (pSUPER-GFP vector) and confirmed knockdown in transfected (GFP positive) neurons through quantitative immunocytochemistry. Expression of SEPT6-shRNA halted axon extension in vitro and also the protrusion of filopodia and lamellipodia (data not shown).

(B) In ovo electroporation studies

The award allowed us to purchase an in ovo elctroporation unit and we have been developing this method and using it in preliminary investigations. Figure 6 shows an example of an embryo transfected with a GFP expression vector. GFP labeling is seen throughout the peripheral nerves and is absent from surrounding tissues in the limb. We have also been able to culture explants from transfected embryos and we obtain a 50-60% transfection frequency (# transfected axons/total axons). This approach will greatly enhance our current Amaxa Nucleofection-based transfection method which requires dissociated cells and results in much lower transfection rates. The ability to obtain high transfection rates and culture the neurons in the form of explants will expedite later experiments on guidance by providing a more favorable geometry of axon outgrowth for guidance studies (e.g., interaction of growth cones with substratum-border or beads coated with attractants (e.g., NGF).

We have used this approach to express GFP-SEPT6, GFP-SEPT7 and SEPT6-shRNA in vivo. Transfection is performed at day 3 or development, by technical requirements. At this stage dorsal root ganglia have not yet commenced axon extension. In preliminary work analyzing the distribution of axons in embryo whole-mounts on embryonic day 5 and 7 we find that SEPT6-shRNA blocks axon extension in vivo (consistent with in vitro results, see above) (Figure 7B). Overexpression of SEPT6 did not have overt effects on axon extension or guidance, but a more detailed analysis will be performed using histological analysis of axon distribution (not shown). At a qualitative level, overexpression of SEPT7 appears to promote axon branching in preliminary experiments (Figure 7C). We are currently commencing additional experiments which will be followed by a quantitative analysis of branching.

We have also been able to perform live imaging of growth cone dynamics in vivo using GFP-actin expression (Figure 8). Imaging can be performed on superficial sensory axons close to the skin in wholemouts using a 100x objective and 6 sec intervals for at least up to 5 minutes. This will allow us to determine effects of experimental manipulations on growth cone dynamics in vivo in future studies.

(C) Submission of extramural proposal

We have submitted an NIH R01 proposal to continue our analysis of the role of septins in growth cone dynamics, axon extension and guidance. The proposal will be revised and resubmitted in the coming year as we accumulate additional evidence in support of the project. Reviewers indicated that the proposal would benefit from additional preliminary data, which continued support from the current award will allow us to generate. Furthermore, reviewers noted as a

weakness that the collaborative team does not yet have any published work on studies of septins in neurons. In the coming year we will be completing and submitting for publication a project detailing the roles of SEPT6 and SEPT7 in axon branching.

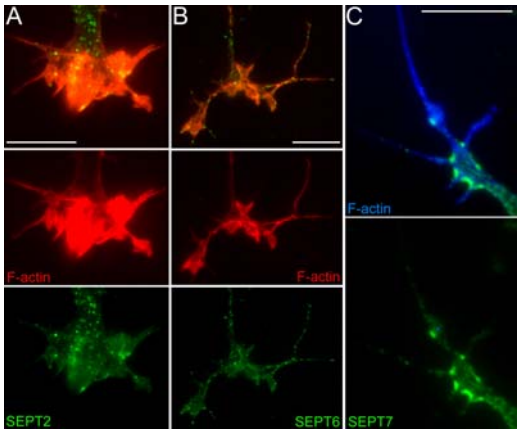

Fig 1. Examples of SEPT2 **(A),** SEPT6 **(B)** and SEPT7 **(C)** staining in growth cones. Bar=10 μm

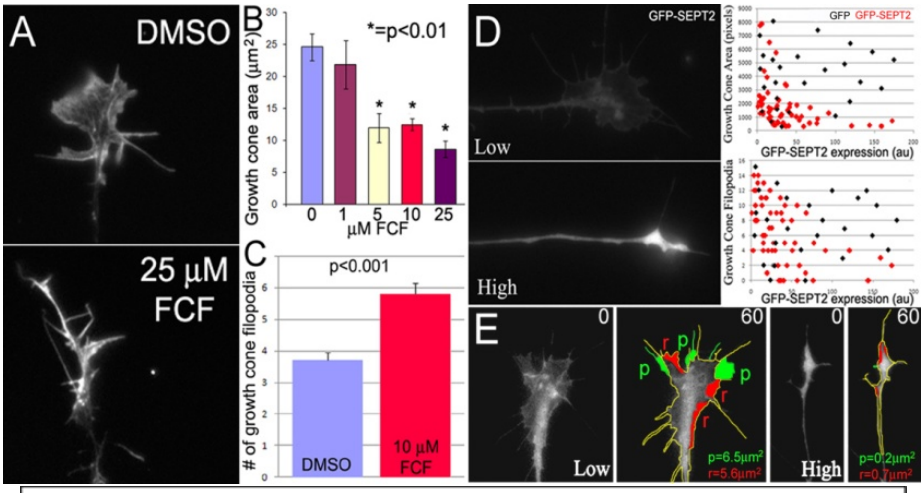

Fig 2. (A) Effects of FCF on growth cones (F-actin shown). **(B)** FCF decreases growth cone area in a dose-dependent manner. **(C)** FCF increases the number of growth cone filopodia. **(D)** Samples of growth cones expressing SEPT2 at low and high levels. Graphs show quantification of growth cone size and number of filopodia as a function of GFP-SEPT2 and GFP expression levels measured in axons. **(E)** High levels of SEPT2 expression (right panels) decrease growth cone dynamics relative to low levels of expression (left panels). Note that image intensity is adjusted for visibility. Images are shown at a 0-60 sec interval. Difference Image analysis: The outline (yellow) of the growth cone at t=0 is overlaid with that at t=60 and areas of protrusion (p; green) and retraction (r; red) are shown. Changes in the surface area protruded (p) and retracted (r) are shown in the t=60 panels.

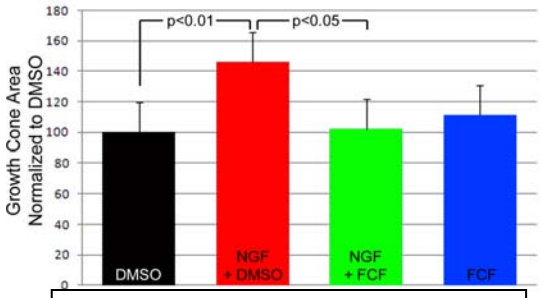

Fig. 3. Pre-treatment with FCF (25 μM) blocks the increase in growth cone area induced by NGF. n≥46/group. Welch t-test.

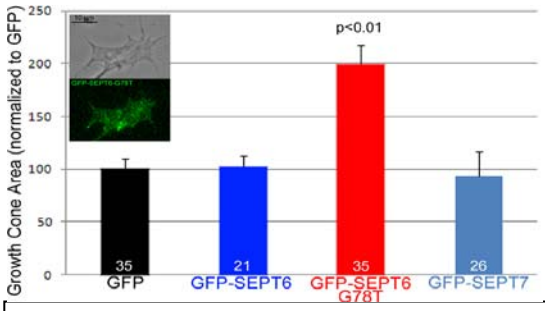

Fig 4. Quantification of growth cone area as a function of GFP and GFP-septin expression. Inset shows example of GFP-SEPT6-G78T-expressing growth cone. n: growth cones sampled, shown in bars.

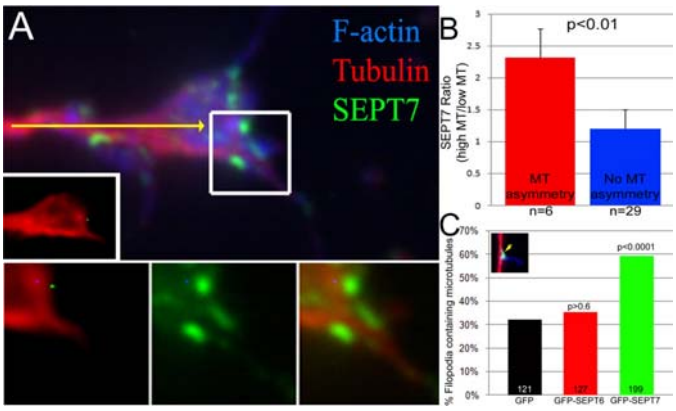

Fig 5. **(A)** Triple labeled growth cone showing F-actin, tubulin and SEPT7. The arrow indicates the axis of the axon. The box shows the region of highest microtubule (MT) content. Lower panels show tubulin and SEPT7 channels in box. **(B)** Quantification of the ratio of total SEPT7 intensity on the side of growth cone containing the highest amount of tubulin to the opposite side (MT asymmetry). In growth cones with no MT asymmetry the "right" side of the growth cone was used as denominator. **(C)** SEPT7 is targeted to the base of axonal filopodia (inset, arrow). Overexpression of SEPT7 but not SEPT6 increases the % of filopodia containing microtubules. n=numbers of filopodia. X^2 analysis on raw data. # in bars = filopodia sampled

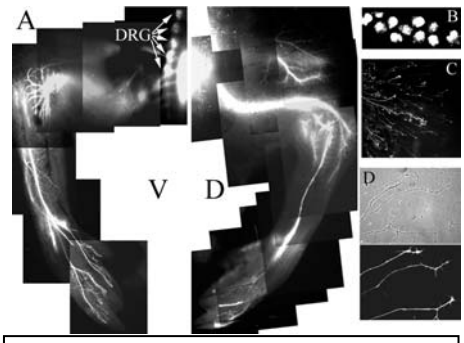

Fig 6. (A) Stage 36 (E9) embryo transfected with GFP. Collage was made from 10x images of the embryo immediately after extraction from its egg. V=ventral, D=dorsal. **(B)** GFP positive DRG explants shown immediately after culturing. **(C)** GFP positive axons 24 hrs later. **(D)** Phase and GFP imaging of axons.

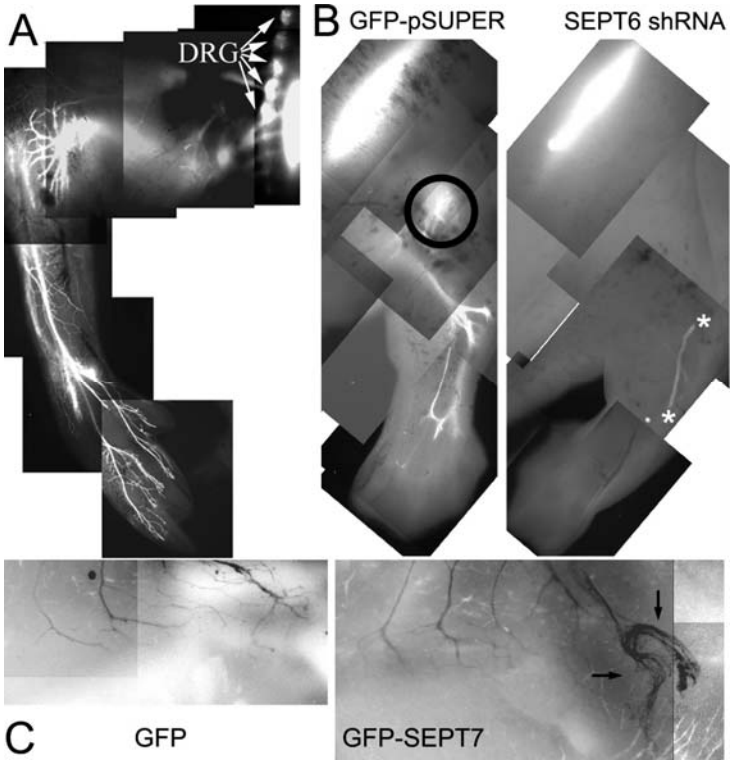

Fig 7. (A) Montage of images taken from wholemounts of the hind limb an E9 embryo transfected with GFP. **(B)** Montages of E7 embryos transfected with GFP-pSUPER or GFP-pSUPER SEPT6 shRNA. Dorsal nerve bundles are clearly visible in the limb of the GFP-pSUPER control but absent in the shRNA expressing embryo. The structure between * is a contaminating autofluorescent fiber. **(C)** Higher resolution montage of axons in the superficial dorsal lateral femoralis cutaneous nerve of E7 limbs (circled in B). Preliminary observations indicate that GFP-SEPT7 expression increases terminal branches and can result in pronounced increases in terminal aroborization (arrows). Images are inverted to increase contrast.

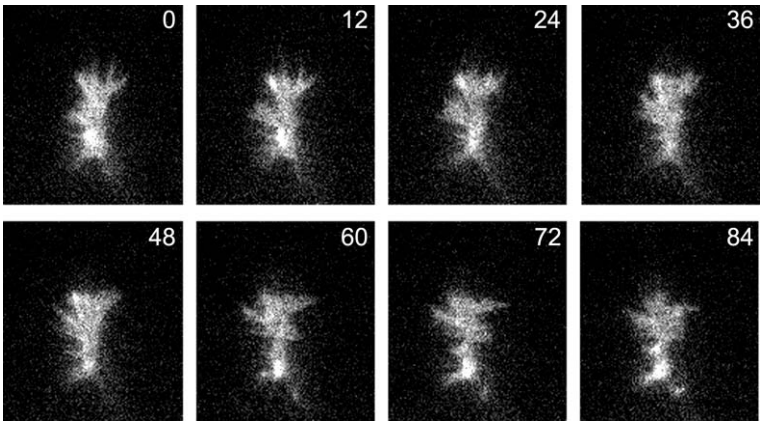

Fig. 8. In vivo imaging of GFP-actin in sensory growth cones. Timelapse sequence shows a growth cone sampled every 6 sec. Numbers in panels denote seconds lapsed from frame 0.

Research Project 5: Project Title and Purpose

Development of the Cardiac Ultrasound Pacemaker - There is an unmet need for a technology to reliably and painlessly pace the heart without any surgical implantation or intravascular catheter placement. Our objective is to develop a technology that would provide noninvasive, low infection risk, and reliable pacing for minutes to weeks in conscious patients requiring temporary or emergency pacing. We envision an ultrasound device that could be placed directly on the skin of the chest wall that would function as a pacemaker for the heart.

Anticipated Duration of Project

1/1/2010 - 12/31/2010

Project Overview

We will research and develop a completely non-invasive, fully ambulatory, and safe alternative pacing technology using externally applied ultrasound at FDA approved frequencies and intensities. The applied ultrasound device will be able to initiate periodic myocardial depolarization resulting in cardiac contraction thereby establishing a consistent and reliable pacing rhythm without need for the direct or indirect application of electric energy. In contrast to all other devices on the market, the technology proposed in this development effort is completely extracorporeal; an external, wearable ultrasound pacemaker.

A porcine model will be used for our experiments. The choice of a porcine model is supported by the literature since pigs and humans share similarities in terms of the anatomical heart size, location and position of the heart in the thoracic cavity, and intrinsic heart rate. Moreover, these animals will be available for noninvasive testing at our institution. Porcine heart rhythm will be monitored using surface electrodes and a multi-channel electrocardiogram. An M-mode ultrasound imager will be used to identify a location on the chest wall that provides access to the myocardium with a minimum of obstructions. The external ultrasound probe will be placed on the chest surface with coupling gel. The ultrasound pulses will be synchronized with the native heart rhythm using an electrocardiogram to avoid inducing ventricular arrhythmia. Following FDA guidelines, only ultrasound intensity levels with a spatial peak temporal average of 720mW/cm2 or less will be used for the feasibility studies. For the feasibility studies ultrasound pulses will be delivered for one minute, at a pulse interval approximately 25% below the inherent cycle length, to initiate pacing at 20 beats per minute (bpm) faster than the average underlying heart rhythm of 70bpm. The ultrasound-initiated beats will be identified by the morphology of their QRS complexes and timing relative to the ultrasound pulse. A successful pacing protocol will be defined by a 70-100% capture of the delivered ultrasound pulses for three to five minutes. This will provide data on 270-450 successive stimulations for analysis. The heart rhythm will be monitored with the electrocardiogram for an additional 5 minutes to document whether any residual electrophysiologic effects from the ultrasound are present.

Principal Investigator

Andrew R. Kohut, MD, MPH

Assistant Professor of Medicine
Drexel University College of Medicine
Mail Stop 470
245 North 15th Street
Philadelphia, PA 19102-1192

Other Participating Researchers

Peter A. Lewin, PhD - employed by Drexel University
Peter B. Kurnik, MD, Steven P. Kutalek, MD - employed by Drexel University College of Medicine
Christopher Vecchio, PhD - employed by Spectrasonics Imaging, Inc.

Expected Research Outcomes and Benefits

Cardiac pacemakers have been in existence for almost 50 years. There are two categories of cardiac pacemakers, temporary and permanent. The most recent statistics indicate there are about 1.3 million temporary cardiac pacemakers used annually in the USA at a total cost of about $3.4 billion dollars. Globally, the figures are much higher. The two current techniques for temporary cardiac pacing involve the surgical use of intravascular catheters and leads or the use of transcutaneous electrical pacing, which is painful and impractical for prolonged utility. These approaches have not significantly changed in the last 40 years and are associated with a myriad of morbidity and mortality outcomes as well as high costs. Complications can include infection, drug toxicity, renal failure due to prolonged use of antibiotics, and death.

Our proposed ultrasound device will operate at intensities that follow current FDA guidelines. It will provide rapidly-deployable, noninvasive, painless pacing for minutes to weeks in conscious patients requiring temporary or emergency pacing. Temporary cardiac pacemakers often represent the first therapeutic approach for the ultimate correction of a serious cardiac problem or malady. Such situations often result from bradyarrhythmias myocardial infarction, drug toxicity, bloodstream infection, during patient transport in emergency situations, or in the aftermath of heart surgery. The medical complications and costs associated with current approaches represent a very poorly met medical need, ripe for improvement both in terms of clinical outcome and cost reduction. As a result of the development of the proposed technology, the need for painful and invasive temporary intravascular pacing catheters or transcutaneous electrical pacers would be reduced or eliminated.

Summary of Research Completed

We have assembled an experimental cardiac ultrasound pacemaker system and have begun conducting preliminary animal experiments using the system. A diagram of the system appears in Fig. 1. The system uses a 1.6MHz 15mm diameter unfocused transducer and is synchronized to the native cardiac rhythm. Custom gating hardware was designed to detect the QRS complex and deliver the pacing bursts of ultrasound during precise time intervals following each QRS peak (i.e. during ventricular depolarization). The gating hardware was used for two reasons: it allows us to deliver pacing pulses at a rate somewhat greater than the native rhythm in order to

demonstrate the induced pacing effect and, because it prevents the application of pacing pulses during the QRS complex, it lets us avoid inducing tachyarrhythmias via potential early afterdepolarizations (EADs) and delayed afterdepolarizations (DADs) . The transducer used in the experiments conducted to date is shown in Fig. 2. Two other custom transducers (shown in Fig. 3) have been constructed recently and will be used in future experiments. The new 1.6 MHz transducer is acoustically and electrically identical to the transducer shown in Fig. 2 but is mounted in a more compact case which will make it easier to maneuver and position. The second transducer is of the same form factor but operates at 2.5MHz. We will be acquiring additional transducers in the near future to allow us to test the technique at a number different frequencies. Fig. 4 shows the predicted ultrasonic energy deposition as a function of frequency and skin-to-heart distance. This graph suggests that for an expected anatomical distance of approximately 5 cm, the optimal frequency will be around 0.8MHz. Experiments will be conducted in the frequency range of 0.5MHz to 2.5MHz in order to verify this.

A preliminary series of experiments was performed on 2 porcine models available at our institution utilizing a protocol approved by our University's Institutional Animal Care and Use Committee (IACUC). The following protocol was used for both animals:

1. Placed 3 ECG electrodes on the shaved chest wall of anesthetized animal
2. Connect ECG electrodes to the stimulating ultrasound and gating hardware
3. Place ultrasound transmission gel and ultrasound probe on chest wall
4. Synchronized ultrasound pulse delivery to native heart rhythm to avoid inducing ventricular arrhythmia. The native porcine heart rate was slightly higher than anticipated, approximately 120-140 bpm.
5. A fixed frequency ultrasound probe of 1.6 MHz was applied using Aquasonic 100® ultrasound transmission gel at approximately the midaxillary line at the level of the 6-8th intercoastal space.
6. Ultrasound bursts were delivered over one minute intervals, using delays of 0.15, 0.2 and 0.3 seconds (corresponding to target heart rates of 400, 300, and 200 BPM respectively) following the peak amplitude of the QRS complex. The pulse durations were set at 2, 4 and 8 milliseconds, while targeting a sound pressure level of 2.5-3.5MPa (megapascal) at the site of stimulation.
    a. Ultrasound bursts delivered:
        i. 1.6 MHz with pulse delay of 0.15 sec and pulse duration of 2 msec
        ii. 1.6 MHz with pulse delay of 0.15 sec and pulse duration of 4 msec
        iii. 1.6 MHz with pulse delay of 0.15 sec and pulse duration of 8 msec
        iv. 1.6 MHz with pulse delay of 0.20 sec and pulse duration of 2 msec
        v. 1.6 MHz with pulse delay of 0.20 sec and pulse duration of 4 msec
        vi. 1.6 MHz with pulse delay of 0.20 sec and pulse duration of 8 msec
        vii. 1.6 MHz with pulse delay of 0.30 sec and pulse duration of 2 msec
        viii. 1.6 MHz with pulse delay of 0.30 sec and pulse duration of 4 msec
        ix. 1.6 MHz with pulse delay of 0.30 sec and pulse duration of 8 msec
7. The native heart rhythm was recorded by the 3-lead surface ECG rhythm strip.
8. The ECG rhythm strips were reviewed and analyzed for the presence of ultrasound-initiated beats after each ultrasound pulse parameter change.

9. The heart rhythm was monitored with the electrocardiogram for an additional 5 minutes to document whether any residual electrophysiologic effects from the ultrasound were present.

These preliminary experiments did not result in any clearly identifiable ultrasound-initiated beats as determined by a review of the recordings. The transducer used in these initial tests was likely to have been a contributing factor - its size and shape made it difficult to position accurately on the chest wall and may also have resulted in inconsistencies in ultrasonic coupling. We have made several system upgrades in response to this lack of mechanical capture. As described above, we have designed and constructed two new ultrasound probes with an improved form factor and will be purchasing additional probes that will allow us to operate at different (potentially more favorable) frequencies. We have acquired a new power amplifier (ENI model 3100LA) and signal generator (Agilent model 33220A) that will greatly enhance our ability to broaden the ultrasound exposure matrix and have purchased a new ECG monitor that will provide a clearer signal with a decrease in signal artifact, allowing us to more precisely gate our ultrasound delivery. The rapid native heart rate (up to 140 bpm) encountered in the preliminary experiments may also have interfered with our ability to induce additional beats. We have rewritten the animal protocol to allow for us to utilize different anesthetic agents to provide deeper sedation in an effort to prevent anxiety and associated increased heart rates in our porcine models. This new animal protocol will also allow for a broader and more comprehensive protocol per each porcine model as total experiment time with each animal has been extended to 4 hours, as well as, multiple protocols being performed on each animal. This revised animal protocol has been submitted to the IACUC committee for review on July 14, 2010.

We are currently in the modification stage of our series of experiments. With our initial prototype and animal protocol we identified several problematic areas/components and are in the process of addressing these issues. The next series of experiments is expected to begin within a couple of weeks of IACUC approval.

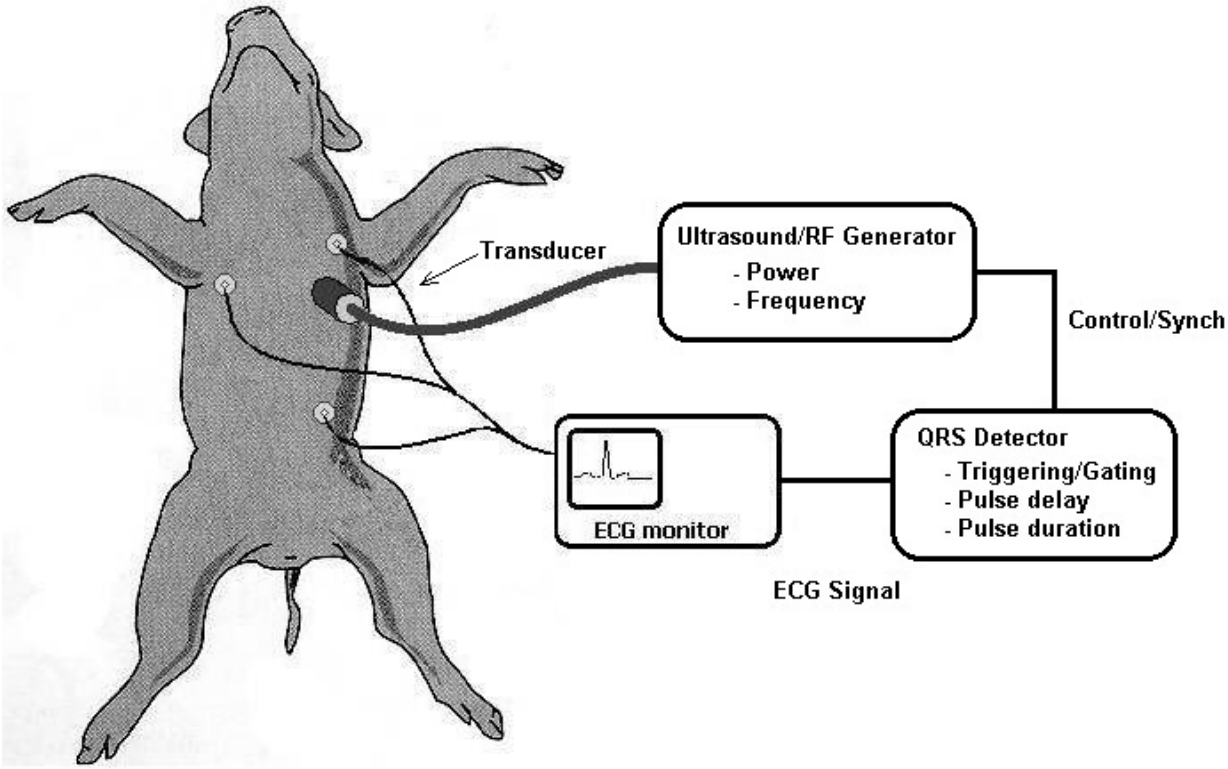

Fig. 1. Diagram of Cardiac Ultrasound Pacemaker experimental system.

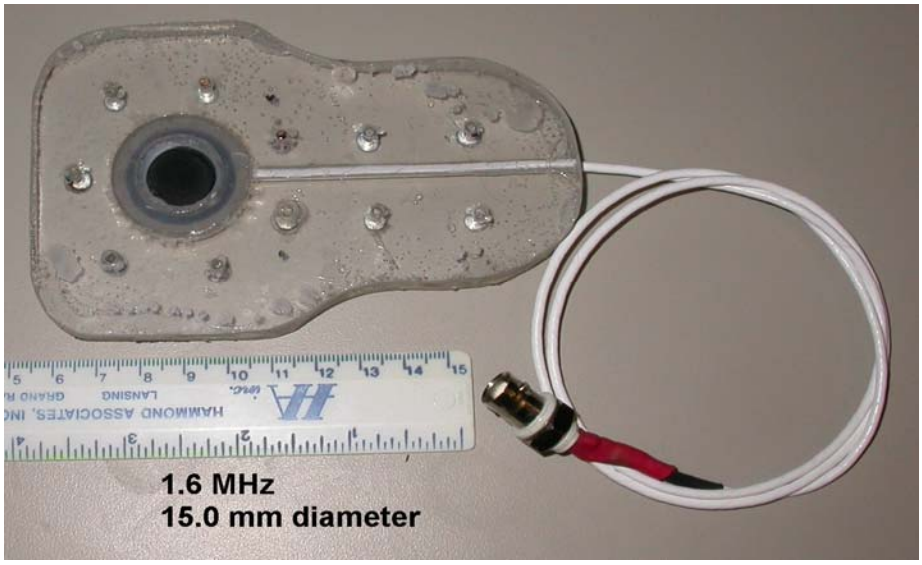

Fig. 2. Unfocused, 1.6MHz, 15mm diameter transducer used in the experiments conducted to date.

Fig. 3. Unfocused, 1.6MHz, 15mm diameter and 2.5MHz, 10mm transducers which will be used in upcoming experiments.

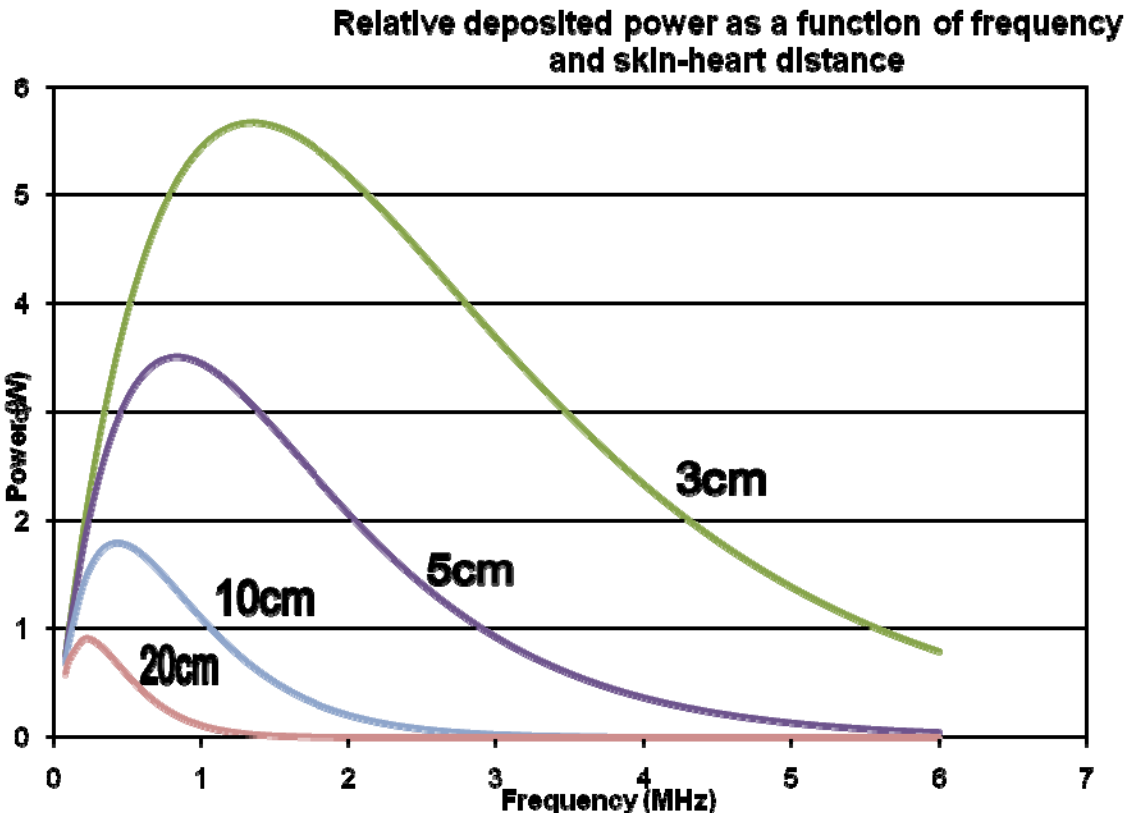

Fig. 4. Predicted ultrasonic energy deposition into a 0.5 cm thick heart wall at distances of 3, 5, 10, and 20 cm from the skin surface as a function of frequency. Peak energy deposition for the 5cm curve occurs at a frequency of approximately 0.8MHz.

Research Project 6: Project Title and Purpose

Human Lung Progenitor Cells for Pulmonary Tissue Engineering and Regenerative Medicine - The purpose of this interdisciplinary research is to isolate and study human lung-specific somatic progenitor cells. These cells can be used to engineer high-fidelity distal pulmonary constructs (alveolar forming units, AFUs) for studying basic mechanisms of lung development and ultimately, for treating currently incurable lung diseases, such as in newborns (e.g., pulmonary hypoplasias) and/or in adults , e.g. chronic obstructive pulmonary disease (COPD), such as emphysema. Moreover these AFUs can also lead to a commercializable tissue-engineered product for use as models in accelerated drug discovery (e.g. improved anti-asthmatics), in understanding common lung infections (e.g. pneumonia/tuberculosis), or in toxicity studies (e.g. asbestos/vapor inhalation).

Anticipated Duration of Project

1/1/2010 - 12/31/2010

Project Overview

Project goals will be achieved through three specific aims:

Aim1: *To isolate and characterize human lung progenitor cells (hLPCs) derived from distal airways/alveoli.* Using techniques established in non-human mammalian lung, we will isolate, culture and characterize hLPCs from freeze-thawed fragments of human distal lungs, obtained from anonymous donors from the Tissue Bank.

Aim 2: *To develop an optimized regimen for the directed differentiation of hLPCs into diverse distal pulmonary alveolar cells.* The main goal of Aim 2 is to develop an optimized regimen for the directed differentiation of hLPCs into diverse distal pulmonary alveolar cells, specifically AE2 cells and endothelial cells (ECs) and other mesenchymal cells.

Aim 3*: To assess assembly of hLPC into "alveolar forming units" upon seeding into tissue-engineered permissive matrices*. In this aim, we will explore the functional assembly of hLPC derivatives into vascularized, surfactant synthesizing "alveolar forming units", similar to our prior work with fetal murine lung cells as a model system

In this project we will synergistically leverage the unique expertise of two laboratories in an effort to propel Drexel to the apex of personalized lung tissue engineering and regenerative medicine. Moreover the availability of tissue samples (biopsies) from individual patients opens the realm of "personalized" regenerative medicine, the possibility to study patient-centered lung development in health and disease and/or producing autologous lung cells for transplantation back into the patient.

Principal Investigator

Peter I. Lelkes, PhD
Calhoun Chair Professor of Cellular Tissue Engineering
Drexel University
3141 Chestnut Street, Bossone Room 707
Philadelphia, PA, 19104

Other Participating Researchers

Edward S. Schulman, MD, PhD - employed by Drexel University College of Medicine

Expected Research Outcomes and Benefits

We fully expect to be able to isolate spore-like pulmonary stem cells, to be able to differentiate these stem cells toward pulmonary lineages, and to reconstruct distal airways (alveoli like structures), structurally and functionally.

Summary of Research Completed:

Currently there is no consensus in the literature about the existence of an adult stem cell located in the lung that can differentiate into both conducting airway epithelium and alveolar epithelium. There have been reports of whole lungs from mice, rats, and sheep being digested and finding a cell deemed to be an "adult stem cell". The problem with these reports is that most of the papers only show that the cells they have isolated differentiate into conducting airway epithelium, or express markers of such epithelium. Hence, they have isolated a cell that should be called a "Conducting Airway Epithelium Progenitor".

In order to identify adult stem cells, located in lung tissue, which could differentiate into alveolar epithelium, we began our studies by attempting to replicate the work of others. After hiring a graduate PhD student, Mr. Collin Stabler, for this project, our initial goal was to teach him how to digest rodent and human lung tissue in order to obtain the highest yield of general lung cell populations and then to focus on the special cell population that might harbor the "adult" alveolar progenitor/stem cells. Following a careful literature survey and trying out, with mixed success, some of the divers, sometimes opposing protocols, we finally decided to develop our own methodology, by combining several individual methods in order to make a "workable" protocol that was deemed worthy by my superiors. For the sake of availability all initial studies were carried out with adult rat lung. Since there is no consensus in the literature as to what is the best method to digest lung tissue, we went through a fair number of optimization steps (e.g., varying the concentration of enzymes, types of enzymes, as well as the digestion times). At this time, we now have in our hands a reproducible protocol that yields large number of mixed populations of primary adult rat lung cell isolates.

Details of our protocol are as follows:

1.) Intact rat lungs, preferable with intact vascular pedicles are harvested, washed in PBS, and transported in PBS + Pen/Stre to maintain sterility.
2.) The trachea is discarded, and the lungs are finely minced in PBS + Pen/Strep on top of ice for ~10-15min.
3.) The resultant tissue fragments are spun at 200rpm for 5min, and then re-suspended in fresh enzyme solution (1 U/ml Collagenase + 10 mg/ml Elastase), incubated in a shaking water bath and periodically triturated at 37oC for up to 45min.
4.) At various time points of enzymatic digestion (5, 10, 15, 30 and 45 min) the cell suspension is strained through a 70um cell strainer to collect "liberated" cells at various phases of enzymatic digestion. The remaining tissue fragments are then re-suspended in fresh enzyme solution. The supernatant from each of the fractions is strained through a 40um cell strainer, centrifuged at 1000 rpm for 5min, and re-suspended in culture media.
5.) Each cell suspension is then differentially plated for 30 min on gelatin-coated flasks to remove rapidly adhering mesenchymal cells (fibroblasts),
6.) The non-adhered cells are collected, plated and then cultured in a humidified 5% CO2 incubator at 37°C.

Based on the morphology of the resultant cell cultures, this protocol yields different populations of constituent cells; by choosing the right cell culture conditions post isolation, we hypothesize that we can enrich these cultures for alveolar type II epithelial cells and/or the appropriate epithelial progenitor cells. The above protocol yields whole lung populations, after one week in culture, as seen in Figure 1. Specifically, we have identified several culture conditions in which, through addition or omission of serum and specific growth factors, we can selectively modulate the cellular phenotypes.

Based on microscopic/morphologic analysis, we surmise that under optimized conditions the resultant attached cells attain an epithelial phenotype, the unattached rounded cells are reminiscent of stem/progenitor cells growing on a tissue specific feeder layer. We are currently in the process of testing our hypothesis by analyzing these cells by flow cytometry and immunocytochemistry, using lung specific markers.

Having successfully completed his qualifying exams in the early part of the summer, Collin Stabler is now working full time on a three-pronged approach to isolate and characterize the progenitor cells from rats, mice and humans. With the understanding that whatever can be gleaned from rodents (easier and more regularly available than human tissue) will be amenable to application to the humans system. In order to ascertain that the putative distal lung progenitor cells are indeed the elusive "Bronchio-Alveolar Stem Cells", the following modifications have been introduced in the human tissue isolation protocols:

1. Perfusion of tissue with collagenase / elastase before digestion
2. Hypotonic lysis of red blood cell after enzymatic digestion and filtering.

In the next set of experiments we will use magnetic cell sorting to select for the population of interest. Most recent studies suggest that this population is characterized by being CD45-, CD31, Sca1+, CD34+. Once isolated and characterized the alveolar epithelial phenotype will be ascertained by flow cytometry and immunofluorescent staining using as consensus markers (CCSP+, SP-C+).

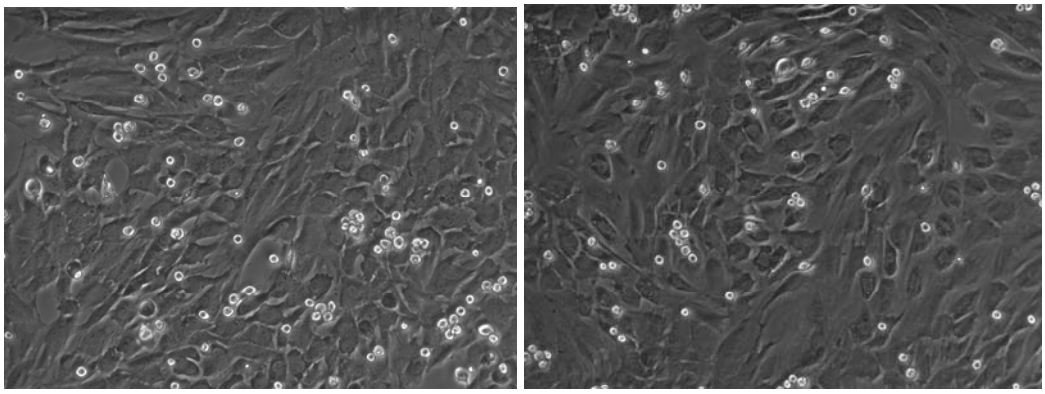

Figure 1: Primary adult rat lung cell isolates, enriched for epithelial cells and putative progenitor cells

Research Project 7: Project Title and Purpose

Novel Oligomers Targeting AMPA Receptors as Therapeutics for ALS - In this project we will evaluate the efficacy of compounds we have developed called splice modulating oligomers (SMOs), which dramatically decrease flip/flop levels of targeted GluR AMPA subunits, to improve motor function and prolong lifespan in transgenic ALS mice. SMOs are compounds that function by binding to their target pre-mRNA, and redirecting pre-mRNA splicing by the spiceosomal complex in a predictable fashion. Due to recent improvements in chemistry, SMOs show extraordinary specificity, potency, and resistance to degradation. We propose that our SMOs could ultimately be used clinically as neuroprotective agents for treating amyotrophic lateral sclerosis (ALS), by reducing calcium influx in motor neurons (MNs) and breaking the feedback cycle involved in glutamate-mediated excitotoxicity.

Anticipated Duration of Project

1/1/2010 - 12/31/2010

Project Overview

Amyotrophic lateral sclerosis (ALS) is characterized by the progressive and selective loss of motor neurons (MNs) in the motor cortex, brainstem, and spinal cord, resulting in patient death typically 3-5 years after diagnosis. Glutamate-mediated excitotoxicity in the CNS has been firmly implicated as a major contributor to the manifestation of both sporadic and familial ALS. Excitotoxicity is the result of excessive Ca2+ influx into MNs, coupled with the diminished capacity of MNs to handle Ca2+ overload, which appears to result in excessive Ca2+ entering mitochondria and the release of harmful molecules from mitochondria, which appear to damage glutamate transporters on adjacent astrocytes. This sets up a disastrous feedback cycle in which synaptic glutamate levels continually rise, further increasing Ca2+ influx and exacerbating mitochondrial Ca2+ overload, ultimately leading to MN cell death. Therefore, drugs which effectively lower Ca2+ influx in the MNs during excitatory activity offer great promise as therapeutics for ALS.

In this project we will evaluate the efficacy of our lead SMO after continuous ICV delivery to reduce GluR3-flip isoform expression in relatively short-term 3 wk trials in ALS mice; focusing on the dose-response of GluR3-flip knockdown throughout the CNS. We will then conduct longer-term ICV delivery trials of the efficacy of our lead SMO in ALS mice; focusing on delaying motor deficits and increasing lifespan.

Principal Investigator

Gordon J. Lutz, PhD
Associate Professor
Drexel University College of Medicine
245 N. 15th St.
New College Building, MS 497
Philadelphia, PA. 19102

Other Participating Researchers

Melanie K. Tallent, PhD, Terry Heiman-Patterson, MD, PhD - employed by Drexel University

Expected Research Outcomes and Benefits

We will evaluate the efficacy of our lead SMO after continuous ICV delivery to reduce GluR3-flip isoform expression in relatively short-term 3 week trials in ALS mice; focusing on the dose-response of GluR3-flip knockdown throughout the CNS.

We will also conduct longer-term ICV delivery trials of the efficacy of our lead SMO in ALS mice, focusing on delaying motor deficits and increasing lifespan.

The proposed experiments are all empirical in nature and are product-driven with the express intent to provide 'proof of principle' that our novel drug candidates are efficacious in improving motor function and lifespan in an animal model of ALS. There are no drugs in clinical usage that specifically decrease AMPA channel GluR-flip subunit expression or increase desensitization kinetics. The SMOs in this project may ultimately be used clinically as neuroprotective agents for treating ALS, by reducing Ca^{2+} influx in MNs and breaking the feedback cycle involved in glutamate-mediated excitotoxicity.

Summary of Research Completed

<u>Establishment of Alzet cannula/pump system for ICV delivery in mice</u>
Because splice modulating oligomers (SMOs) do not cross the blood-brain-barrier, for studies in adult mice it is necessary to use a continuous intracerebroventricular (ICV) SMO delivery system. During this report period we successfully worked out the mechanics of continuous ICV delivery of SMOs using the Alzet cannula/minipump system. We found using fluorescently-tagged SMOs that the stereotaxic coordinates and methods of cannula and pump implantation were adequate to achieve widespread distribution of SMO throughout the CNS (not shown). In another set of experiments, residual volume was measured in pumps implanted at 90 days and

explanted at 118 days. We found residual pump volume to be within 1-2% of the expected volume (N = 10 mice). These data demonstrate that SMO delivery rates to the lateral ventricle were extraordinarily reliable.

ICV delivery of GluR3 SMO reduces GluR3-flip levels throughout CNS of normal mice
Normal mice were implanted with cannulae in their lateral ventricle connected through small tubing to subcutaneous implanted Alzet minipumps containing various concentrations of the GluR3-flip SMO. The GluR3 SMO dosing rates were set to 1, 10, and 20 μg of SMO per day for 3 weeks of continuous ICV delivery, and GluR3-flip transcript levels were measured using Real-time PCR (Figure 1). These data clearly indicate that continuous ICV delivery of the GluR3 SMO, for only 3 weeks, produced remarkable reductions in the level of GluR3-flip transcripts throughout the CNS. Specifically, SMO doses from 1 to 20 μg/d decreased the level of GluR3-flip expression. Importantly, a dose as low as 10 μg/d decreased GluR3-flip transcripts in all regions of the CNS to between 10-40% of the saline controls, even in the cervical and lumbar spinal cord.

ICV delivery of GluR3 SMO improves motor function and longevity of ALS mice
ALS mice were administered GluR3 SMO (10 μg per day) for 8 weeks by continuous ICV delivery using the Alzet cannula/minipump system, beginning at 90 days of age, when tremor and other signs of neuromuscular pathology are apparent. SMO-treated ALS mice showed a significant increase in lifespan (172.9 ± 2.4 d; N = 8) compared to the saline-treated (161.3 ± 5.5 d; N = 6) and untreated (160.7 ± 2.8 d; N = 7) mice (Figure 2). The mean age of survival for the untreated ALS mice of 162 days is in close agreement with previous reports. The SMO-treated mice also showed a marked improvement in upward ladder climb (Figure 3).

In the above experiments the second pump was explanted at 146 days of age, and the cannula was capped and left in place. These data demonstrate that our ALS mice will tolerate an additional pump replacement at 146 d of age, which will allow for continuous ICV delivery of SMOs much closer to the point of endstage in the ALS mice, which will likely produce additional improvements in motor function and lifespan.

In summary, our findings from a single SMO and dosing regimen suggest SMO-mediated functional improvements in ALS mice, and overall, our data firmly establish feasibility of our experimental approach.

Evaluation of potential adverse effects of continuous ICV delivery of SMOs on cognition and motor function in normal mice
In pilot studies we evaluated the influence of 4 weeks of continuous ICV delivery of our GluR1 SMO (10 μg/day) in normal mice beginning at 110 days of age. Although the data are too preliminary to establish statistical significance, we found no differences between SMO and saline-treated mice in motor function tests including splay, beam walk, grip strength, ladder climb, and wire suspension (data not shown; N = 3 mice per group). Additionally, no differences were found between SMO and saline-treated mice in novel object recognition or object displacement tests, indicating normal cognition.

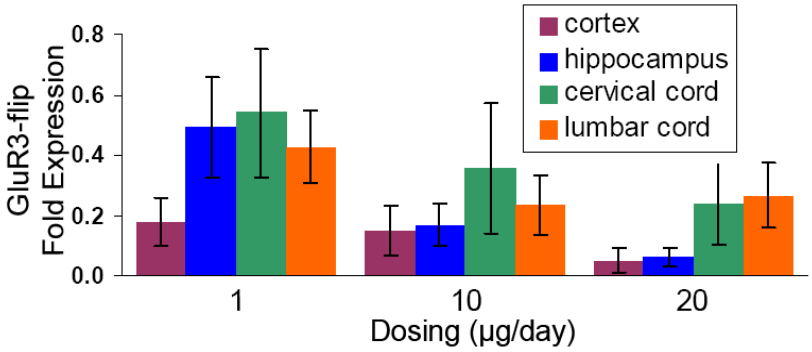

Figure 1. Dose-response of GluR3-flip knockdown in CNS of mice following ICV delivery of GluR3 SMO. GluR3-flip transcript expression is markedly reduced in brain and spinal cord of adult B6 mice after 3 weeks of continuous ICV delivery of the GluR3 SMO using the Alzet/cannula system (N = 4 mice per group).

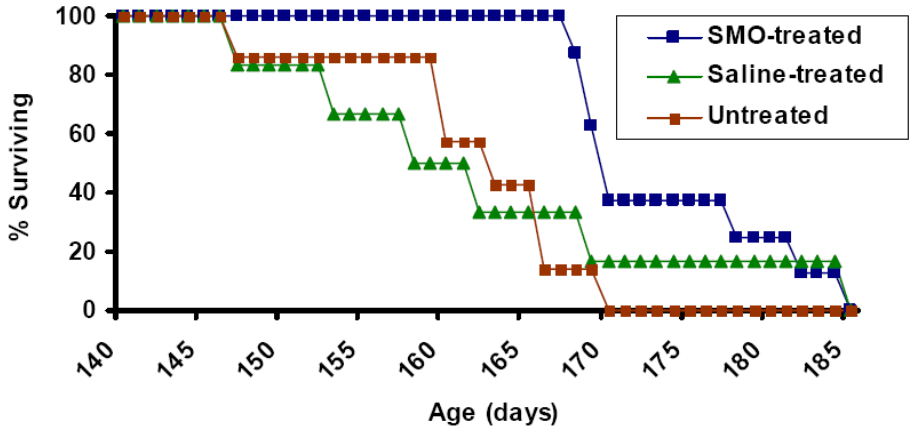

Figure 2. Kaplan-Meyer analysis of lifespan of ALS mice. Mice were administered GluR3 SMO (10 µg per day) for 8 weeks by continuous ICV delivery using the Alzet cannula/minipump system, beginning at 90 days of age. SMO-treated ALS mice (N = 8) showed a significant increase in lifespan compared to the saline-treated (N = 6) and untreated (N = 7) mice.

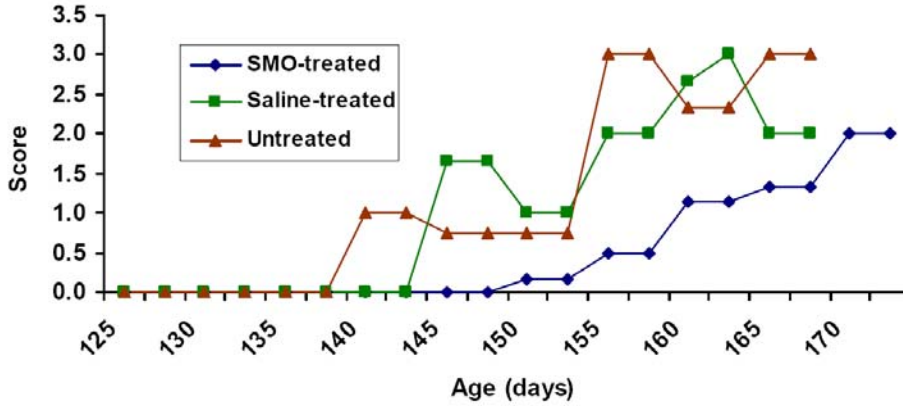

Figure 3. ICV delivery of GluR3 SMO markedly improved upward ladder climbing ability. Ladder climbing ability was ranked on a scale of 0-3 with criterion as follows: 0 = mouse can climb to the platform in < 30s without slipping or falling, 1 = mouse can climb to platform in <30 s with intermittent slipping, 2 = mouse can climb to platform within 30-60 s with slipping and signs of exhaustion, and 3 = mouse cannot climb apparatus.

Research Project 8: Project Title and Purpose

Neuronal Substrates of Cognitive Flexibility - Cognitive flexibility is the capacity to alter behavior to meet unexpected challenges, and is an essential aspect of adaptive behavior. Unfortunately, deficits in this capacity are hallmarks of various psychological and neurodevelopmental disorders including schizophrenia, obsessive compulsive disorder, and autism. Furthering the development of effective treatments for individuals with these disorders requires a more comprehensive understanding of the physiological processes mediating behavioral adaptability. The overarching aim of this project is to develop a novel experimental paradigm to explore the detailed neurophysiological substrates of cognitive flexibility using the laboratory rat as an experimental model.

Anticipated Duration of Project

1/1/2010 - 12/31/2010

Project Overview

Our general aim is to investigate the neurophysiological substrates underlying the ability of rats to flexibly adapt their behavioral strategy in an effort to acquire rewards. Our hope is that knowledge gained from this project will facilitate the further development of pharmacological and behavioral interventions aimed at treating disorders that compromise cognitive flexibility, such as schizophrenia, obsessive compulsive disorder, and autism.

Current evidence suggests that the prefrontal cortex and striatum work in concert to flexibly guide behavioral output toward adaptive ends. We will record single neuron activity from these two regions in awake, behaving rats as they employ multiple strategies in a visual discrimination task for rewards. In our first Aim, we will train rats to discriminate between two visual patterns,

each presented to either the right or left side. Subjects will be required to indicate the location of the target of interest by releasing one of two response levers with one of their forelimbs. Our second aim is to extend this paradigm to investigate the neural correlates of attentional set-switching, the ability to select and focus on a subset of available sensory information to guide behavioral decisions. This will constitute a test of cognitive flexibility which has been shown to be influenced by medial prefrontal cortex. Ultimately, our goal is to successively introduce two additional attributes to the visual patterns: luminance (normal or bright) and visual stability, where each pattern will either remain steady or flicker. Subjects will be trained to empirically identify and selectively attend to the one of the three stimulus dimensions which is relevant to obtaining reward (ex., releasing the lever corresponding to the appropriate pattern, while ignoring differences in luminance and stability). For the period covered under the present funding, we plan to begin training subjects on one additional dimension: luminance.

Prefrontal cortex is thought to encode behavioral rules relevant to achieving goals, while neurons in the striatum are known to respond to goal-directed forelimb movements and to sensory stimuli that elicit these movements in trained animals. We will study the neuronal activity underlying the ability to alter behavioral strategies to achieve goals as external environmental demands (task rules) change. We hope these studies will lead to a better understanding of how neurons in the prefrontal cortex and striatum reorganize their activity to accommodate changes in task requirements.

Principal Investigator

Jeffrey T. Oristaglio, PhD
Research Assistant Professor
Department of Pharmacology and Physiology
Drexel University College of Medicine
245 N. 15th St.
Philadelphia, PA 19102

Other Participating Researchers

Jed S. Shumsky, PhD - employed byDrexel University College of Medicine

Expected Research Outcomes and Benefits

Severe rigidities in both thoughts and actions result from a variety of neurodevelopmental and psychiatric disorders. Such behavioral abnormalities are debilitating to the afflicted individual, often stunting the development of social interactions and language skills. For family members and caregivers, they are often a source of frustration and hardship, and can ultimately present a significant impediment to the effective treatment of the underlying disorder. The goal of this project is to better understand how the brain mediates the flexibly adaptive goal-directed behavior which is characteristic of normally-functioning individuals. Particularly, we wish to understand how the brain modifies behavioral strategies to respond to changing environmental circumstances, and how these strategies are used to formulate appropriate goal-directed behaviors. We will develop a series of novel studies to investigate the neurophysiological

substrates of cognitive flexibility in rats trained to selectively attend to changing stimulus-response contingencies on a reward-based visual discrimination task. The proposed studies are timely, as new and potentially useful rat models of neuropsychiatric disorders such as Obsessive-Compulsive Disorder, Attention Deficit Disorder, and Autism are being developed and tested. A thorough characterization of the differences in brain activity underlying properly adaptive and cognitively rigid behaviors will provide a biomarker with which to assess the likely efficacy of putative therapeutic compounds. If realized, our project objectives will productively extend the investigative options of researchers interested in studying important aspects of executive function, thus facilitating the further development of ongoing translational research aimed at developing treatments for neuropsychiatric and developmental disorders.

Summary of Research Completed

The overarching goal of this project is to better understand the physiological substrates underlying cognitive flexibility: the capacity of animals to alter their behavior in response to changing environmental challenges. We proposed to train rats to perform complex, rule-based visual discrimination tasks in which the strategy required for accessing rewards is changed without warning. Formally, this task bears resemblance to more complex tests used to assess cognitive flexibility in humans, as well as to those used in previous studies of rodents performing in ethological contexts. We also proposed to record single-neuron activity from two brain regions implicated in flexible behavior while rats perform this task: the medial prefrontal cortex (mPFC) and the dorsolateral striatum (DLS). In the first six months of the award period, we have taken five significant steps toward achieving this goal: 1.) A laboratory technician with experience in behavioral training of rats was hired and began working in the lab. 2.) Equipment and software for experimental control of visual discrimination tasks (Med PC, Med Associates) was purchased, assembled, and interfaced with the existing neuronal recording system. Core software for behavioral control, performance monitoring, and data analysis has been written, tested, and implemented in pilot behavioral studies (see below). 3.) A pilot histological study was conducted to confirm that brain regions of interest could be consistently reached based on previously published coordinates. 4.) We have worked to develop a novel cranial implant technique which will allow for head immobilization and multiple single-neuron recordings, performed bilaterally, from multiple brain regions (we are continuing to develop this technique). 5.) We have begun computer-automated training of three subjects to perform a simple visuo-spatial cueing task which will serve as a prelude for training on more complex visual discrimination tasks. Details of the experimental procedures and findings resulting from these projects are discussed below.

Since it takes considerable time, on the order of several months, to train subjects to perform the complex tasks required for this project, our rats have grown considerably, and are roughly twice the size of rats used in other published studies utilizing neurophysiological recordings. Therefore, we were concerned that previous published coordinates for the brain regions of interest would not result in correct electrode placements in our subjects. This is also of major concern due to the fact that, once trained, subjects will be experimented with over the course of several months. Should electrode placements be incorrect, this would result in considerable misdirected effort. To address this issue, we undertook a histological study to mark the locations of desired regions of medial prefrontal cortex (mPFC) and dorsolateral striatum (DLS) in 11

subjects ranging from 460-700 grams in weight (comparable to fully grown subjects currently undergoing task training) and subsequently identified marked locations through histological analysis. Subjects were anesthetized with ketamine and xylazine or isoflurane gas and their heads were anchored to a stereotaxic frame (Kopf Instruments). The scalp was then shaved and an incision was made along the dorsal midline to expose the skull. A micro treffin, 2.7 mm in diameter (Fine Science Tools), was used to cut a circular window in the skull (caudal boundary at 0.5-0.7 mm anterior to Bregma and centered on the midline), providing bilateral access to medial prefrontal cortex. Small burr holes were also drilled over each side of the dorsolateral striatum (0.7 mm anterior, 3.7 – 4.0 mm lateral to Bregma). Low impedance metal electrodes were then lowered to appropriate depths at each region of interest. Three locations were marked in mPFC: the rostral and caudal boundaries of the skull opening and the center point of the opening. In this case, we wanted to be sure that our opening spanned a substantial region of mPFC, including the anterior cingulate cortex (ACC). Marks were also made bilaterally in the DLS. Approximately 10 uA of electrode negative DC current was delivered though the electrode for 5-10 seconds, resulting in a small burn mark in the tissue. Subjects were then perfused with physiological saline followed by 10% buffered formalin. Their brains were then extracted and placed in buffered formalin for at least 2 days, followed by 30% sucrose formalin. Coronal sections (60 um in thickness) were made through mPFC and DLS and plated on slides.

Figure 1 displays representative locations of electrode placements in the two regions. Electrode locations were mapped to the nearest coronal diagram in the atlas of Paxinos and Watson (6th edition) based on the location of visible landmarks (nuclei, white matter tracts, ventricles) and the shape of the slice. Generally, electrode placements were well within targeted regions. A small number of exceptions to this were evident: three DLS placements which were directed too far laterally into the white matter of the external capsule. Moving coordinates from 4.0 mm to 3.7 mm lateral to Bregma rectified this problem, as all subsequent penetrations were within the DLS. Only two PFC placements were directed outside of the target area, terminating near or just within secondary motor cortex (M2).

In preparation for behavioral training, we assembled and programmed a basic behavioral control system using the MedPC system (Med Associates). This allows for the presentation of visual images on a computer monitor while concurrently monitoring and recording a subject's behavioral responses (lever presses and releases). So far, we have succeeded in training subjects to perform a simple visuospatial cueing task (Figure 2) which will serve as a prelude for training on pattern discrimination. Subjects initiate a trial by depressing two levers simultaneously, one with each forepaw. After a brief delay, a visual cue, a white square, appears to either the right or left of midline. Subjects indicate the location of the cue by releasing the appropriate lever, while holding the opposite lever down. This task will also provide a behavioral screen for identifying subjects with the ability to learn more complex tasks. Prior to training, subjects were placed on a water deprivation schedule which maintained them within 85-90% of their normal weight when there is free access to water. Prior to each training session, subjects are placed in a small restraint box located approximately 20 cm from a computer monitor. The subject's forelimbs are allowed to rest on two steel response levers (Coulbourn Instruments, Whitehall, PA), placed at the floor of the restrainer. A programmable infusion pump (Coulbourn Instruments model E73-02) delivers water (approx. 0.05 ml) for reward to a lick spout in front of the subject's mouth. So far, we have trained our subjects without head fixation since the undue stress of this procedure

can disrupt learning. The initial stages of task training have proceeded in multiple phases. Subjects were first trained to press and hold two levers down for a reward. Gradually, the duration of lever pressing was extended. Subjects were then trained to release one lever in response to a manual cue, such as touching one paw with a cotton swab. As subjects learned to consistently respond to this cue, they began releasing prior to contact (i.e., to the sight of the object approaching their paw). Gradually, presentations were made at increasing distances in front of the subjects until they were proficient at responding exclusively to the sight of the object. Subjects were then exposed to the presentation of visual cues on the computer screen, and were proficient at generalizing to this new context. Computer-controlled automated training began shortly after, with the experimenter supervising but not directly participating in training. It has taken 5-8 weeks to train each subject to a level of performance that permits automated training.

To date we have been training three rats to perform this task. Figure 3A shows the percentage of correct trials for one subject during one session of training (268 completed trials; L: left paw, R: right paw, B: both paws). Figure 3B displays response latencies of this same subject. Figures 3C and D show data for another subject (234 completed trials) trained to a higher level of performance. Notice that subject 1 (3 A and B) displays faster response latencies but a lower level of performance than subject 2 (C and D). This is consistent with a more impulsive behavior, a characteristic that the first subject has displayed throughout training. These discrepancies between subjects are of particular interest to us in relating neural signals to reaction time and learning ability. The third subject (data not shown) has, to date, been trained to a lower proficiency but still exhibits above chance performance. Subjects performing this task to criterion (80% correct or better) will be implanted and accommodated to head fixation. We will test their ability to switch from the visually-cued strategy to a motor-specific strategy: releasing either the right or left paw regardless of the position of the visual cue.

We have also developed a novel surgical technique for performing multiple single-neuron recordings in head-fixed subjects (Figure 4). All surgeries were performed under sterile conditions and in complete accordance with the regulations of the Drexel University IACUC and the American Veterinary Medical Association (AVMA). Subjects were anesthetized with isoflurane and positioned on a stereotaxic frame (Kopf Instruments model 930) with non-traumatic ear bars (Kopf Instruments, Tujunga, CA). A micro treffin, 2.7 mm in diameter (Fine Science Tools), was used to cut a circular window in the skull, centered on Bregma, providing bilateral access to medial prefrontal cortex. A 3mm diameter threaded plastic cylinder (Plastics-1) was centered over the hole and anchored with dental cement. Small burr holes were drilled over each side of the dorsolateral striatum (anterior 0.8 – 1.0 mm, lateral 3.6 – 4.0 mm from Bregma) and guide cannulae (Plastics One, Roanoke, VA), were lowered into place over the dura and anchored to the skull with dental acrylic. Four stainless steel bone screws were inserted into burr holes in the skull as anchors for the implant. An indexable tooling set screw was then embedded horizontally at the back of the implant, allowing head position to be anchored with metal posts attached to a stereotaxic frame (Kopf Instruments).

We have obtained high-quality, single-neuron recordings from two head-fixed subjects (Sprague-Dawley rats) sitting at rest in a small restraint box. Subjects were sedated (ketamine-xylazine) and allowed to fully awaken with their heads immobilized and electrodes in place. Figure 5

shows a representative recording from somatosensory cortex of one subject with a cannula implant (somatosensory cortex overlies the striatum at this level). As these were naïve subjects, they sometimes struggled for short periods in an attempt to free themselves. We were able to maintain excellent recordings on well-isolated neurons despite these movements.

Finally, we are nearing completion of a second experimental system that will allow us to test freely-moving rats for their ability to perform complex visual discriminations. This system will provide a high-throughput screen for new rats that can perform our tasks.

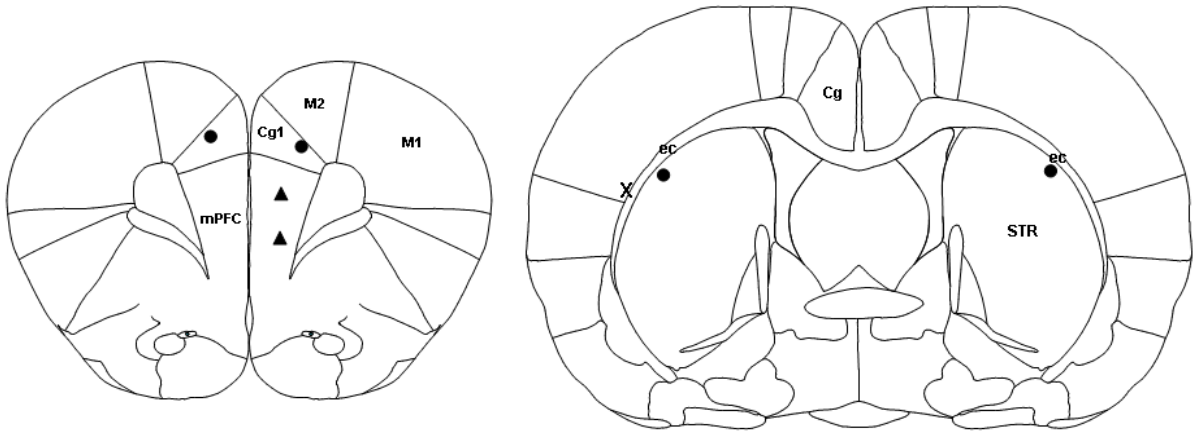

Figure 1: Representative electrode placements. *Left*: sample placements into cingulate (circles) and medial prefrontal cortex (triangles), approximately 3.2 mm rostral to Bregma. *Right*: representative markings in dorsolateral striatum. Some early placements were directed too far lateral (X) into the whitematter of the external capsule. Cg: cingulate cortex, mPFC: Medial prefrontal cortex, M1: primary motor cortex, M2: secondary motor Cortex, STR: striatum, ec: external capsule. Diagrams of coronal sections from Paxinos and Watson, The Rat Brain in Stereotaxic Coordinates, 6th ed., 2009, Academic Press.

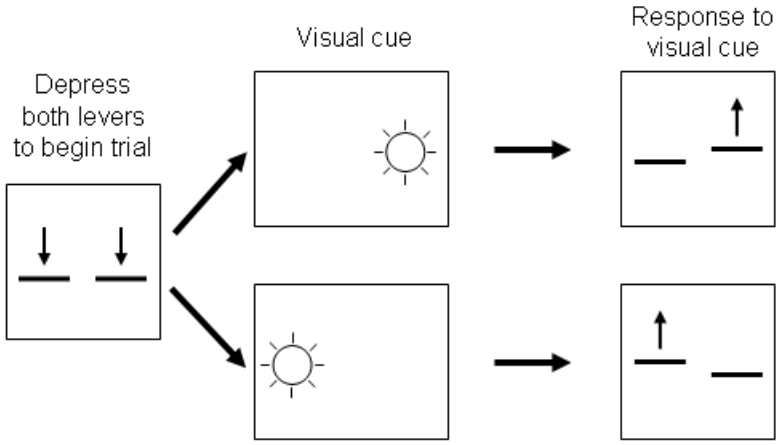

Figure 2: Visuospatial cue task. A trial begins when subjects depress (downward arrows) both levers (horizontal lines). After a short delay, a visual cue, a white light on a black background, appears to one side of space. Subjects are rewarded for releasing (upward arrows) the lever corresponding to the side of space where the cue appears. After learning this task, subjects will be accomodated to head fixation and tested with a rule change requiring the release of one of the two levers (right or left) regardless of where the cue appears. Large arrows depict the flow of time.

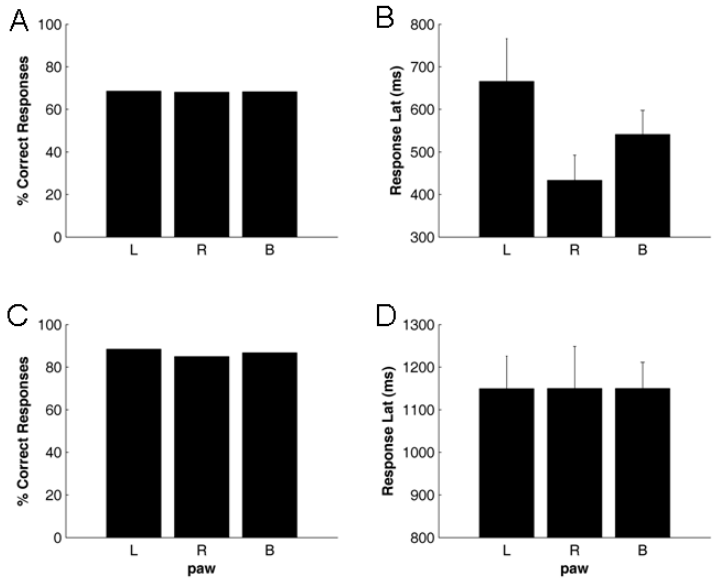

Figure 3: Behavior of two subjects in the visuospatial cue task. (A,C) Percentage of correct responses for subject 1 and 2, respectively. (B,D) Mean response latencies. L: left paw, R: right paw, B: both paws combined. Mean latency values from correct trials only.

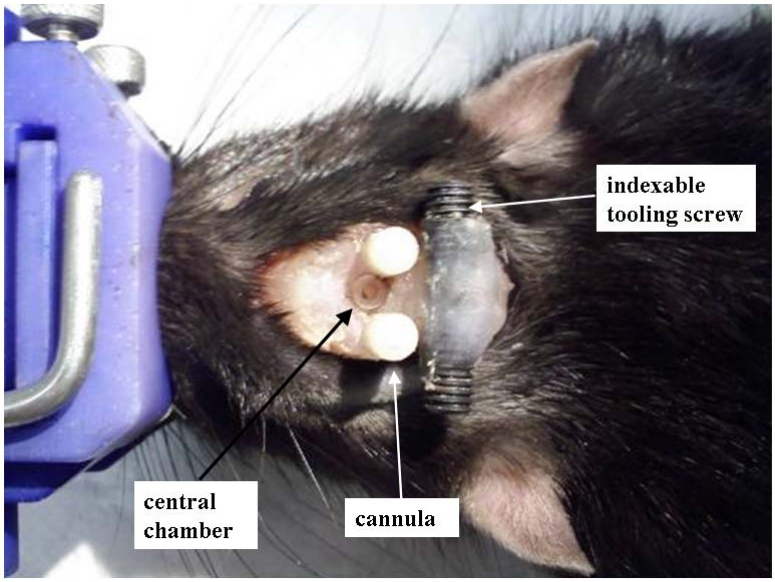

Figure 4: Cranial implant. A centrally located set screw covers a chamber into which recording electrodes can be lowered for access to medial prefrontal cortex. Two 26 gauge stainless steel cannulae (covered by dust caps) flank the central chamber and allow access to the dorsolateral (sensorimotor) striatum. Head immobilization is achieved by threading steel posts with hex key terminals into the indexable tooling screw embedded in the back of the implant.

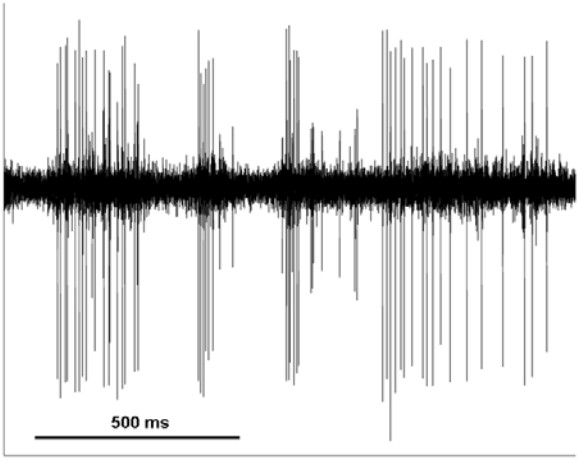

Figure 5: Representative single-neuron recording fromsomatosensory cortex of an awake, restrained subject. Action potentials from multiple neurons can be clearly differentiated. The recording electrode was lowered through a stainless steel cannula with the shaft of the cannula serving as the ground electrode.

Research Project 9: Project Title and Purpose

Microfabricated QLISA Biosensor with Embedded Heating and Mixing Elements – The purpose of this project is to develop a novel, low cost microfabricated poly (methyl methacrylate) (PMMA) Quantum-dot-Linked-ImmunoSorbent-Assay (QLISA) biosensor with embedded mixing elements. The significant advantages of this microfluidic platform with integrated electrokinetic mixing are: *a)* Higher optical detection sensitivity *b)* Improved detection limit *c)* Higher signal to noise ratio *d)* Reduction of assay *e)* Multiuse system - repeated use of the sensor is possible, and *f)* Platform technology – can be used to detect any biomarker. The bioassay platform developed will use only 1-2 microliters of sample and achieve detection sensitivity of picomolar quantities of antigen.

Anticipated Duration of Project

1/1/2010 - 12/31/2010

Project Overview

The broad research objective of this project is to develop a novel, low–cost all plastic microfabricated biosensor with embedded mixing elements. *The specific research aims* are 1) Design, fabrication, and testing of a polymethyl methacrylate (PMMA) microchannel for Quantum-dot-Linked-ImmunoSorbent-Assay (QLISA), 2) Enhanced sensitivity by physical and chemical modification of the channels, and 3) Incorporation of electrokinetic mixing onto the PMMA microchannel.

Aim 1: Design, fabrication, and testing of a PMMA microchannel for QLISA
Rectangular microchannels with a width of 100-300 µm, a depth of 10-50 µm, and a length of 2 mm will be fabricated on thin (1-2 mm) PMMA substrates by hot embossing. The substrates will then be bonded via thermal fusion bonding to flat PMMA substrates that have been machined to have inlet and outlet holes. Carboxyl groups (COOH) required for immobilizing antibodies will be induced on PMMA chips via UV assisted selected area functionalization.

Aim 2: Enhanced sensitivity by physical and chemical modification of channels
Physical modification: Excimer laser (ArF, 193 nm) ablation will be used to create diverse microstructures (grooves, pillars, grids, wavy surfaces, etc.) on the bottom of the PMMA microchannels. *Chemical modification:* PEI, a cationic amine-bearing polymer, will be used to chemically modify the PMMA channel surface. These modified PMMA microchannels will be directly used for immobilizing antibodies specific to Myeloperoxidase (MPO).

Aim 3: Incorporation of electrokinetic mixing onto the PMMA microchannel
Among several electrokinetic mixing techniques the electrothermal effect has been identified as the optimal approach for the current application. Rotational flow patterns due to electrothermal effect will be achieved via interdigitated gold microelectrodes in the PMMA microchannel. These planar microelectrodes will be fabricated on flat PMMA substrates using the lift-off technique. The rotational flow can be observed under a microscope via the motion of

microbeads suspended in the solution. Finally, the effect of electrothermal mixing on the sensor performance will be evaluated through actual QLISA assays for MPO.

Principal Investigator

Elisabeth S. Papazoglou, PhD
Assistant Professor
Drexel University
School of Biomedical Engineering
3141 Chestnut Street
Philadelphia, PA 19104

Other Participating Researchers

Hongseok (Moses) Noh, PhD, Sundar Babu Nadarajan, PhD – employed by Drexel University
Sreekant Murthy, PhD – employed by Drexel University College of Medicine

Expected Research Outcomes and Benefits

The project will develop a sensitive cost effective immunoassay as a platform technology for adoption into many health care fields. The biomarker chosen to validate the technology is a ubiquitous inflammatory marker present in heart disease and in many auto-immune disorders. Health status will be improved because tests can be run on small samples, faster and more economically. The applications for this technology include public health emergencies where a point of care fast test is critical to assess the effect of a biohazard or an infectious disease in the population. Neonate care where sample size is critical can benefit from a test that can give an answer with 1 to 5 microliters of a sample.

The proposed research emphasizes collaboration and development of junior faculty. It will lead to increasing the number of new investigators and by developing stronger grant applications the number of funded grants awarded to the State of Pennsylvania. New products will be developed that can attract new companies to be formed to further commercialize the technology. Since QLISA has been originally funded by the Coulter foundation, business and community involvement is present and can be seamlessly transferred to the innovations developed in the proposed grant.

Summary of Research Completed

Aim 1: Design, fabrication, and testing of a PMMA microchannel for QLISA - Completed

Thermoplastic Microfluidic Device Fabrication: We selected hot embossing as the preferred method to develop our prototype polymethylmethacrylate (PMMA) microchannel design, because a single mold insert can be rapidly manufactured and enable fast and reproducible manufacture of PMMA microchannels. A 2.5” square copper mold insert with raised microstructures was made (via photolithography and electroplating) and these raised microstructures were then transferred to the PMMA substrate via hot embossing to create

microstructures within the PMMA substrate. Lastly, the device was sealed using a solvent assisted bonding technique. An overview of this process is presented in Figure 1 and a more detailed description of this process is provided in what follows.

Photolithoraphy: The fabrication process begins with a photomask, which in this case is a clear field mask. A simple photomask was first designed in order to optimize the fabrication procedure and demonstrate proof of concept for subsequent immunoassay reactions. The photomask consisted of microchannels of various widths (50, 100 and 250um) and pitches (5, 7.5 and 10mm) between microchannels. The photomask was first designed using AutoCAD 2010 and sent to Advanced Reproductions for printing. Upon receipt, the thin film photomask was replicated to create a more durable chrome mask. Once the photomask pattern was transferred to a chrome photomask, photolithography was performed on a cleaned 1mm thick 2.5" copper substrate. SU-8 2150 photoresist (Microchem) was then spun onto the substrate at 500rpm for 10 seconds followed by spinning at 17000rpm (300r/s acceleration) for 30 seconds to produce a final thickness of approximately 200um. The copper plate was then placed onto a hot plate and baked at 60°C for 20 minutes followed by a 40 minute bake at 90°C (softbake). The coated substrate was then cooled to room temperature and exposed to 28mW/cm^2 for 17 seconds (476mJ/cm^2). Following exposure, the photoresist patterned substrate was placed onto a hot plate and baked at 65°C for one hour (a latent image of the pattern should not be visible until minutes into the post exposure bake, if a latent image is seen the pattern was likely overexposed). The patterned substrate is then cooled to room temperature and developed for ten minutes in SU-8 developer under manual agitation. The end product (micropatterned SU-8 on copper substrate) is shown in Figure 2.

Electroplating: After manufacture of the SU-8 micropatterned copper substrate, copper electroplating was performed to create raised microchannel structures on the copper substrate. First, the patterned substrate was cleaned extensively with acetone followed by a rinse in DI water and air-dried. The patterned copper plate was then placed into a holder 35cm from a bare copper plate (cleaned with acetone & DI water). The apparatus was then submerged in a copper electroplating solution (200g copper (II) sulfate pentahydrate, 25ml of concentrated H_2SO_4 in 1mL of deionized water) with an applied DC current of 0.2A for 1 hour under stir bar agitation. These conditions represent our optimized methods for producing uniform raised microchannel structures of 120um in height which were measured by surface profilometry.

Hot Embossing & Coupon Sealing: Following fabrication of the micropatterned copper mold insert, hot embossing was performed to create microchannel grooves on the PMMA substrate. 1cm thick PMMA sheets were cut into 2" squares, cleaned and dried. Once clean a piece of PMMA was sandwiched between a glass plate and the copper mold insert and loaded into a Carver heat press. Both the top and bottom platens were then brought into contact with the copper mold insert and glass plate respectively and set to 140°C. Once the temperature of the platens reached 110°C a pressure of 250psi was applied to the PMMA sheet for a period of 5 minutes and then the platens were cooled to room temperature within the press. A second 2" wide, 1cm thick PMMA sheet was soaked in ethanol for 5 minutes, then brought into contact with the molded PMMA piece and loaded into the Carver heat press between two pieces of glass. The platens were heated to 75°C under a pressure of 250psi for 5 minutes. The sealed

microchannel coupon was then immediately removed from the press and the lumen of the channels was rinsed thoroughly with DI water.

Aim 2: Enhanced sensitivity by physical and chemical modification of channels- Completed with available instrumentation – Goal was achieved with chemical modification

In this Aim we focused and completed the chemical modification step. The laser ablation equipment is still being evaluated after its delayed installation at the Drexel Laboratory.

Thermoplastic Microfluidic Device Validation: Once the microfluidic device was successfully designed and manufactured, an initial proof of concept experiment was performed in order to characterize the performance of a sandwich assay for the detection of lactoferrin within the microchannels. In order to perform these experiments, the lumen of the microchannels was modified by covalently immobilizing polyclonal lactoferrin antibodies using a variety of surface functionalization / modification methods. The microchannels served as the substrate for the subsequent assay. Data on the surface coverage of antibodies on PMMA substrates demonstrate that the optimal functionalization density is achieved with PEG functionalization as compared to PEI or EDC/NHS chemistries. Therefore, we offer details of the PEGylation method only.

PEG Microchannel Functionalization: We have developed a novel surface modification technique in order to increase antibody surface coverage within the PMMA microchannels. First, microchannel surface was activated by circulating 1N NaOH at a rate of 100ul/min, for 1 hour at 60°C. Each microchannel was then rinsed with 1X PBS pH 7.4 and 0.2% PEG solution was circulated at 100ulmin for 1 hour). Following a rinse with Tween surfactant and PBS, a 1% glutaraldehyde solution was circulated at 100ul/min for 30 minutes. Following a second rinse, 500nM polyclonal lactoferrin antibody (500nM) was incubated within the microchannels at 37°C for one hour. Each microchannel was then rinsed with 1ml of 0.05% Tween (1X PBS @7.4) followed by a rinse with 1ml of 1X PBS. An overview of this process is shown in Figure 3.

Antibody Surface Coverage: We have quantitatively determined the surface density of antibody coverage by immobilizing Alexafluor conjugated antibodies onto the surface of PMMA channels using the chemistries outlined above. A standard calibration curve was used to quantify antibody coverage. Our results demonstrated that the PEG/glutaraldehyde method achieves 4-fold immobilization of antibody as compared to passive adsorption, 40% more coverage compared to EDC/sulfoNHS functionalization and more than 30% coverage compared to any PEI functionalization.

Lactoferrin Assay Procedure: After antibody immobilization, five microchannels were incubated with lactoferrin antigen at 50, 100, 200, 400 and 800ng/ml respectively for 40 minutes at 37°C (positive control and standard dilutions). The microchannels were washed with 200ul 0.01% Tween followed by a wash with 200ul 1X PBS pH 7.4, and incubated with 100nM QD-Ab solution for 40 minutes at 37°C. After a standard wash the microchannels were imaged using the optical setup shown below in Figure 5. Our results demonstrated that we were able to detect lactoferrin at levels down to 50ng/ml (Figure 6). An additional optical characterization was carried out in order to compare the sensitivity of our previously published capillary setup with

this newly developed microfludic device (Figure 7). These data suggest that the microfludic device has higher sensitivity than the capillary setup (19.5 and 15.7 AU/(ng/ml) respectively).

Aim 3: Incorporation of electrokinetic mixing onto the PMMA microchannel

Electrokinetic mixing was achieved on a glass substrate which would then be bonded to the PMMA channel device manufactured and validated in Aims 1 and 2. We will use the rest of the project period to incorporate the electrokinetic mixing onto a PMMA substrate and assess how the assay is improved.

Electrothermal mixing device: AC Electrothermal Effect (ETE) refers to fluid motion induced by temperature gradients in the fluid in the presence of AC electric fields. It is caused by uneven Joule heating of the fluid, which induces gradients of conductivity and permittivity, and as a result charges in the fluid bulk move under the influence of the electric fields to generate flows. We have developed the ETE device shown in Figure 8. They were fabricated on a silicon substrate by depositing a 200 nm silicon dioxide isolation layer and parallel chromium–gold electrodes. The electrodes (10nm Cr-100nm Au) are 9 mm long and are separated by 60 mm gaps. Although there are four parallel electrodes, only the center two electrodes were used in this application. A Peltier cooler was applied to enhance the ETE. The experiments were conducted in 1X PBS. The conductivity of 1X phosphate buffer solution (PBS) is 1.77S/m. The voltage applied in these experiments ranged from 5Vrms to 10Vrms. Although different frequencies were tested in the experiment, the 200kHz of frequency is the default setting for most of the tests. 2um and 10um polystyrene microbeads were used to observe the motion in fluid.

Demonstration of electrothermal effect (ETE): First of all, ETE is more pronounced at higher ionic strength fluid, e.g., PBS. Another fluid driving force caused by AC electric field, ACEO, is inhibited in such condition. Secondly, because ETE is caused by temperature gradient, ETE can be enhanced by increasing the temperature gradient. By applying a Peltier cooler, electrothermal mixing was improved (Figure 9). Without the effect of the Peltier cooler, the mixing was restricted only to the right side of the electrodes, which are closest to the power supplier. However, after using the Peltier cooler for 1 min, mixing occurred throughout the electrode area covered by PBS. When turning off the cooler for 10 min, mixing returned to its previous stage, i.e. only happening at the right side of electrodes. Due to this behavior, we are confident that the mixing observed was mainly caused by an AC electrothermal effect. Because of electrode resistance the voltage drops and fluid velocity decreases as the distance from the electric source is increased. In addition to the vertical rotation movement on the Y plane, there is lateral movement along the X direction down towards the ends of the electrodes (Figure 10).

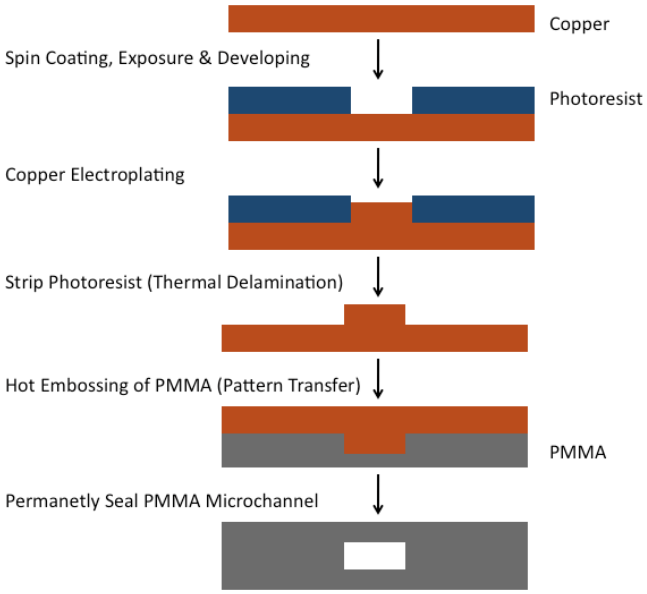

Figure 1: Profile view of the PMMA microchannel fabrication processs. First, the copper is cleaned and patterned with 250u thick negative photoresist (SU-8 2150), creating an active site for copper electroplating in the subsequent step to produce raised microchannel features on a copper substrate (mold insert). The mold insert is then used as a die in the subsequent hot embossing process to produce a microchannel in the desired PMMA substrate. The device is then sealed with a PMMA cover, effectively creating an array of sealed microchannels.

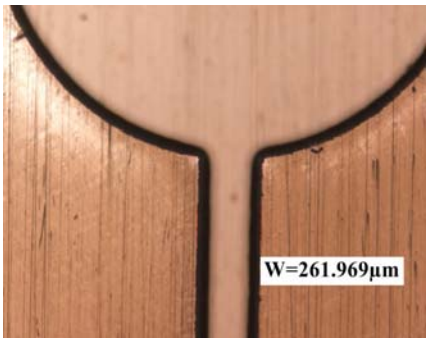

Figure 2: SU-8 patterned copper substrate. The raised SU-8 may be seen on top of the copper substrate. The final width of the microchannel was approximately 260um. The exposed (developed) regions of the SU-8 serve as a substrate for the adhesion of copper during the subsequent electroplating process.

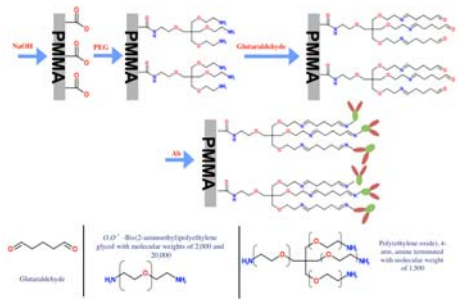

Figure 3.
Overview of PEG functionalization chemistry.

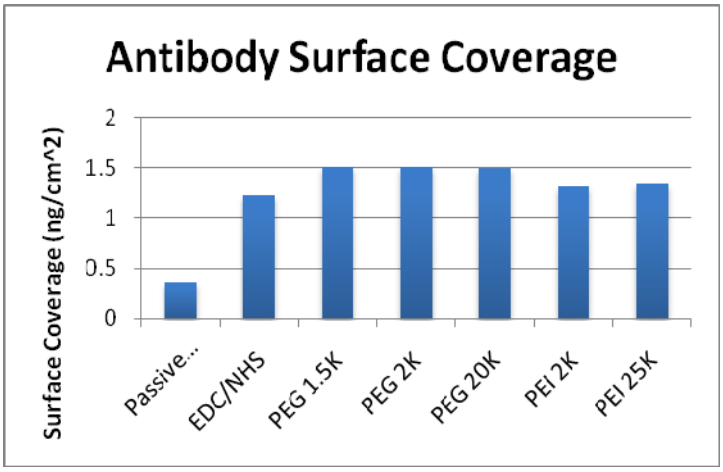

Figure 4: Polyclonal antibody surface coverage in ng/cm^2

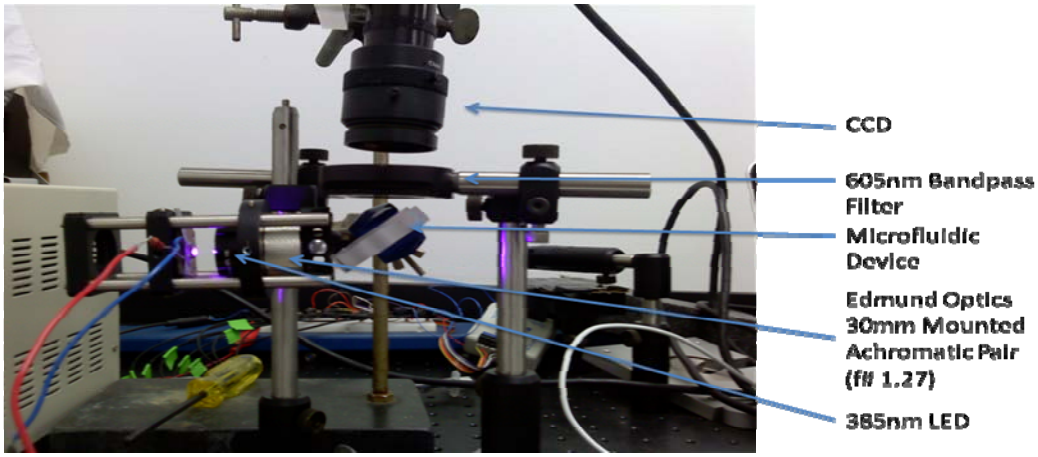

Figure 5: Optical setup designed to detect fluorescence from the PMMA microfluidic channel device.

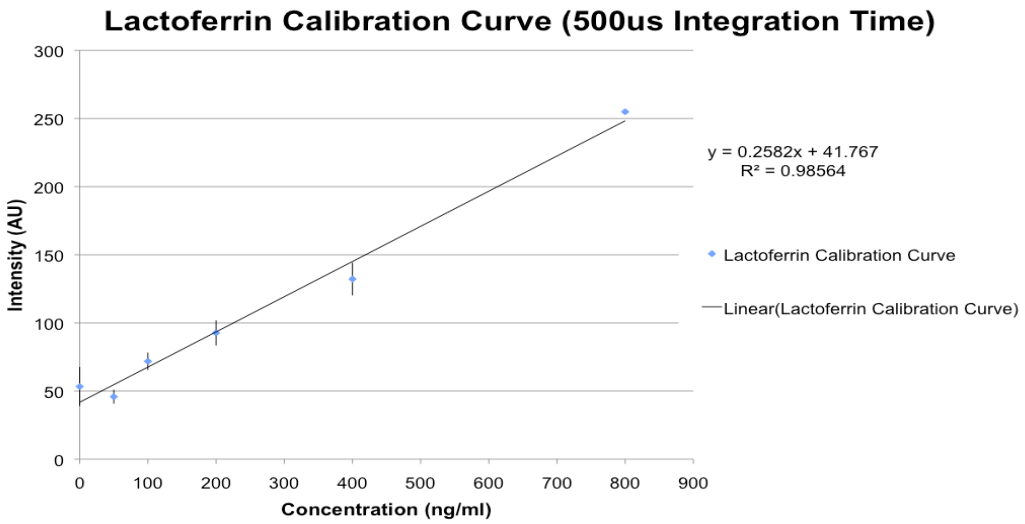

Figure 6: Lactoferrin calibration curve obtained using the microfluidic PMMA platform.

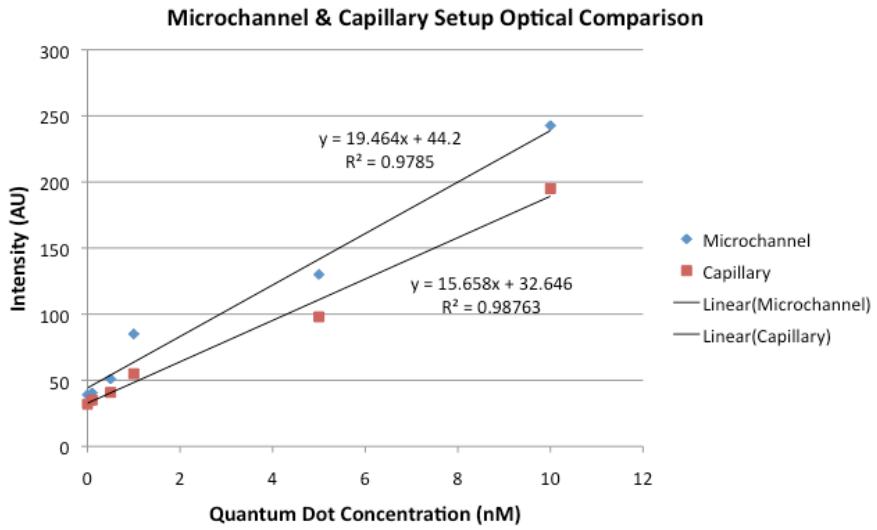

Figure 7**:** Optical comparison of the capillary and microfluidic channel device obtained using quantum dot solutions of varying concentrations

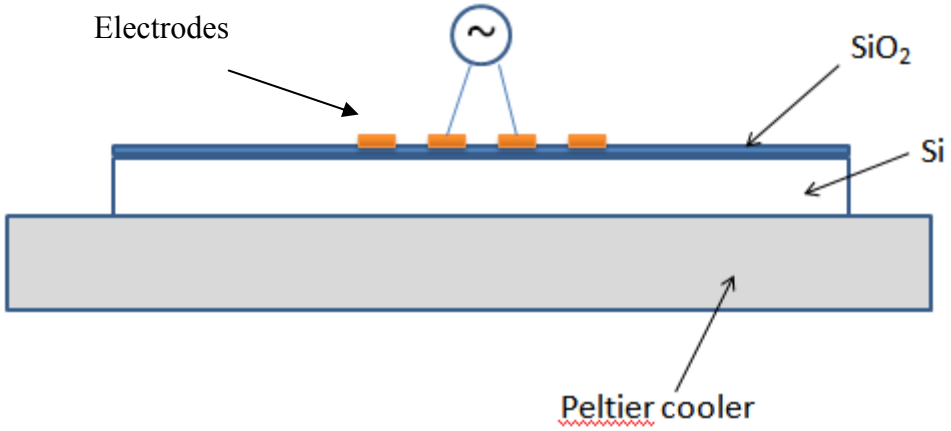

Figure 8: Experimental ETE device. The silicon substrate is isolated with a silicon dioxide layer from Cr-Au electrodes separated by 60 mm gaps.

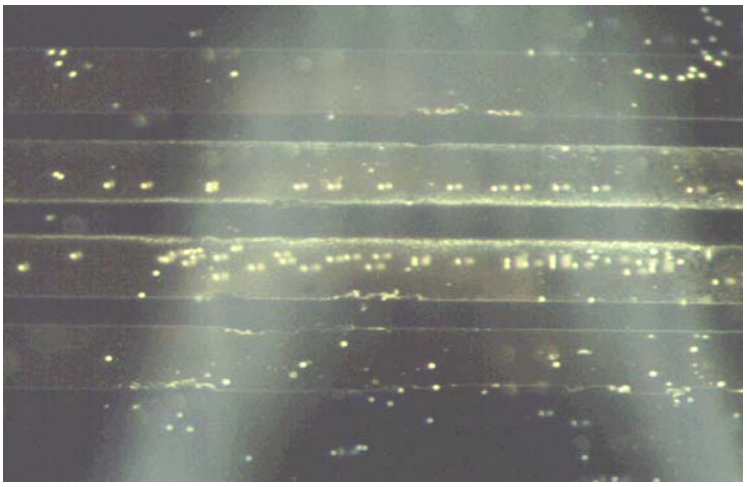

Figure 9: After applying 10Vrms at the middle two electrodes, polystyrene microbeads were attracted by ETE, rotating on two lines.

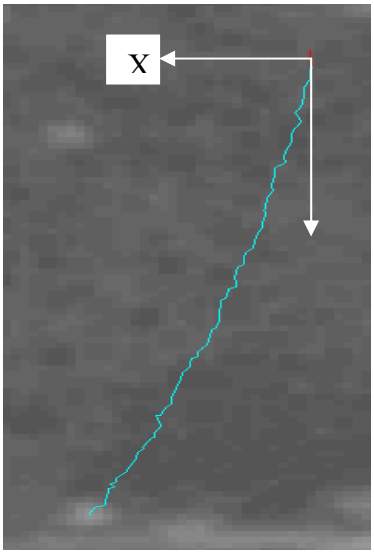

Figure 10: Tracking of the particles by video analysis of images shows that particles rotate on the plane perpendicular to the substrate surface due to ETE, and at the same time, they travel downwards towards the ends of the electrodes because of energy loss along the fingers.

Research Project 10: Project Title and Purpose

The Role of miRNAs in Modulating Alzheimer's Disease Risk - We will test the hypothesis that genetic variation in the 3' untranslated region (3'UTR) of the human amyloid precursor protein (APP) gene may modulate the risk of developing Alzheimer's disease by disrupting miRNA mediated regulation APP levels. The genetic basis of Alzheimer's disease (AD) is not fully understood. Identifying polymorphisms that increase risk will allow for early prediction of who may develop disease. This knowledge may also lead to a novel therapeutic approach to treating AD with molecules that act like miRNAs to decrease APP levels.

Anticipated Duration of Project

1/1/2010 - 12/31/2010

Project Overview

In the past decade our view of RNA has changed dramatically with discovery of non-coding RNAs that regulate gene expression. In particular, microRNAs (miRNAs) function to post-transcriptionally regulate gene expression. miRNAs are RNA molecules 21-23 nucleotides in length that bind to the 3' untranslated region (3'UTR) of messenger RNAs (mRNAs) that have sequences complementary to the miRNA. miRNA binding to this target sequence inhibits translation of the specific mRNA. miRNAs are endogenous negative regulators of gene expression. This function leads miRNAs to be important and even essential regulators of normal cell homeostasis, organismal development, and human diseases. Approximately 800 miRNA genes have been identified in the human genome with a large percentage of these expressed in the human brain.

Emerging evidence suggests that miRNAs may play a role in Alzheimer's disease (AD). The precise mechanisms that cause AD are not completely understood, however proteolytic processing of the amyloid precursor protein (APP) to generate the β-amyloid peptide (Aβ) seems to play a fundamental role in disease pathogenesis. APP is sequentially cleaved by the β- and γ-secretases to generate Aβ, which is known to lead to synaptic dysfunction and give rise to deficits in learning and memory. In AD patients, brain miRNA expression is altered compared to normal aged controls. We recently reported that miR-106a and -520c can regulate APP protein levels. DeStrooper and colleagues then demonstrated that miR-20a, -17-5p, and -106b could also regulate APP levels. Given that trisomy 21 (the human *APP* gene is located on chromosome 21) or *APP* locus duplication are sufficient to cause AD, this suggests that disruption of the miRNA mediated APP regulation may lead to AD.

To test the hypothesis that genetic variation in the 3' UTR of the human APP gene may modulate the risk of developing Alzheimer's disease by disrupting miRNA mediated regulation APP levels, we will (i) identify common polymorphisms in the APP 3'UTR, (ii) test the effect of these polymorphisms on miRNA-mediated regulation, and (iii) determine if these polymorphisms are over-represented in AD patients versus normal, aged controls.

Principal Investigator

Aleister J Saunders, PhD
Associate Professor
Drexel University
3141 Chestnut Street
Stratton Hall
Philadelphia, PA 19104

Participating Researchers

Carol Lippa, MD, Andi Russo, Neha Patel - employed by Drexel University

Expected Research Outcomes and Benefits

The results from this project's experiments will allow us to determine if common genetic variation found in the 3' untranslated region of the human APP gene results in modulation of miRNA mediated regulation of APP levels. This is important since this may reveal a heretofore unappreciated route to developing AD. This would allow for early prediction of individuals that would develop disease, something that is missing for all but the most extreme cases. In addition, the identification of a new mechanism that leads to the development of Alzheimer's disease may also allow for the identification of new approaches for therapeutic intervention.

Summary of Research Completed

We have made significant progress in testing our hypothesis and have strong preliminary data to utilize for submission of an NIH R01 grant anticipated this fall. In addition we will be submitting two manuscripts in the next six months that detail some of this work.

Below we detail the results we have obtained in the first six months of this project.

<u>Aim 1: Identify common polymorphisms in the human *APP* 3'UTR.</u> We utilized two experimental approaches to identify genetic variation in the 3'UTR of *APP*. First we directly sequenced the 3'UTR in families that display genetic linkage on chromosome 21 to AD. Since the *APP* gene is located on chromosome 21, individuals that have disease predisposing or enhancing polymorphisms should be enriched in this sample. The sequencing results for *APP* 3' UTR region in the chromosome 21-linked families revealed no mutations. We extended this 3' UTR sequencing effort to include at least one proband in each family that comprise the entire NIMH sample (n=449). These efforts resulted in the identification of a rare SNP (rs454455403; minor allele frequency 0.021) in one African American family (FAM: 50368) comprising two affected individuals (90C00627- Onset Age=66 & age=71, 90C00782 - Onset Age =57 & age = 72) that are heterozygous for SNP rs45455403. Sequence context of rs45455403 revealed that the polymorphism lies one bp from the predicted seed region of a putative hsa-miR-495 target site (Figure 1A). Sequencing these 449 individuals from the NIMH AD Genetics Initiative sample identified no other polymorphisms. We therefore searched the human genome SNP database for SNPs located in the 3'UTR of *APP*. We identified two other SNPs, rs45541739 and rs1059478 that are located in predicted target sites for miR-376a/b and miR-29a/b/c, respectively. Figures 1B and 1C visualize the sequence context of these SNPs in relationship to the predicted miRNA target site. Interesting, similar to rs45455403, rs45541739 is also only found in African Americans. Together we have identified three polymorphisms that we will test to determine if the minor allele disrupts miRNA-mediated *APP* regulation (Aim 2) and increase risk for developing AD (Aim 3).

<u>Aim 2: Test the effect of these polymorphisms on miRNA-mediated regulation.</u> Given that rs45455403 lies immediately adjacent to the putative miR-495 target site, we tested if this SNP may alter miR-495 mediated APP expression regulation. Using Q-RT-PCR and total brain RNA obtained from a Caucasian male (age = 81 yrs) we confirmed that miR-495 is expressed in normal human brain tissue (Figure 2). Next, we cloned the entire *APP* 3' UTR (containing the major allele "C" of rs45455403) into a position immediately 3' of the firefly luciferase reporter

gene. Co-transfection of this reporter vector in naïve HEK 293 cells along with a miR-495 over-expression vector lead to a significant decrease in luciferase activity (~50% ;$p < 0.001$; Figure 3) compared to reporter constructs where, either the miR-495 seed region was disrupted by mutation or reporter construct lacking *APP* 3'UTR, thus confirming miR-495 can bind to the *APP* 3' UTR and regulate gene expression. Inhibiting the over-expressed miR-495 using a anti-miR-495 inhibitor caused a significant increase in luciferase expression compared to a non-silencing control inhibitor (Figure 4).

Over expression of miR-495 also significantly decreased APP protein levels (~50%; $p < 0.01$; Figure 5) and *APP* mRNA levels (~40%; $p < 0.001$; Figure 6) compared to cells transfected with an empty-vector. Over-expression of miR-106a was used a positive control since it has previously been shown to regulate endogenous APP levels without affecting *APP* mRNA levels. Over-expression of miR-125b had no significant effect on APP levels as expected since *APP* contains no predicted miR-125b target sites. These results demonstrate that the *APP* 3'UTR contains a productive miR-495 target site and can control APP expression levels.

To determine if rs45455403 might alter miR-495 mediated regulation of *APP* expression, we mutated the miR-495 target site within the *APP* 3'UTR to replace the rs45455403 major allele (C) with the minor allele (A) (Figure 7). In addition, we also replaced the rs45455403 major allele with a (T) which should increase complementarity between the target site and miR-495. We co-transfected these luciferase vectors along with a miR-495 over-expression vector in naïve HEK 293 cells and observed that the miR-495 target site harboring the rs45455403 minor allele (A) disrupts miR-495 mediated reporter gene expression observed with the major allele (Figure 8). The miR-495 target site engineered to increased complementarity with a (T) substitution increases miR-495 mediated repression. This allele specific regulation is intriguing given that the major and minor alleles confer no changes in the complementarity between the target site and miR-495.

To gain further insight into the mechanism of this allele specific miR-495 regulation we mutated position 9 of the mature miR-495. This position is analogous to the rs45455403 position in the *APP* 3'UTR in that it is one bp away from the predicted seed region (Figure 9). Mutation of miR-495 resulted in decreased repression luciferase activity compared to wild-type miR-495 (Figure 10). As expected, over-expression of mutated miR-495 also resulted in decreased repression of APP protein levels compared to wild-type miR-495. These results demonstrate that miR-495 position 9 confers complementarity independent specificity to regulation of *APP* miR-495 target site.

We have demonstrated allele specific disruption of miRNA regulation of APP expression. This suggests a novel pathogenic mechanism for AD whereby disruption of miRNA/APP mRNA interaction would lead to increased APP levels and eventually AD. We are currently investigating the effects of rs45541739 and rs35871145 in a similar fashion.

<u>Aim 3: Determine if polymorphisms found in the predicted miRNA target sites of *APP* are over-represented in AD patients versus normal, aged controls.</u> Given the strong functional data in Aim 2 we set out to determine if rs45455403 was over-represented in AD patients compared to controls. rs45455403 is found almost exclusively in the African American community. Since

African American AD research cohorts are rare we have begun to recruit African Americans into our study. We started collecting samples two months ago and to date have collected 14 blood samples, 11 from individuals affected with AD and 3 from individuals unaffected. We have isolated DNA from these samples and just begun the genotyping process. At this rate of collection we should have no issues collecting the number of samples that we propose. In addition to this we are also trying to establish collaborations with other neurology services throughout Philadelphia and the commonwealth to increase the number of samples collected.

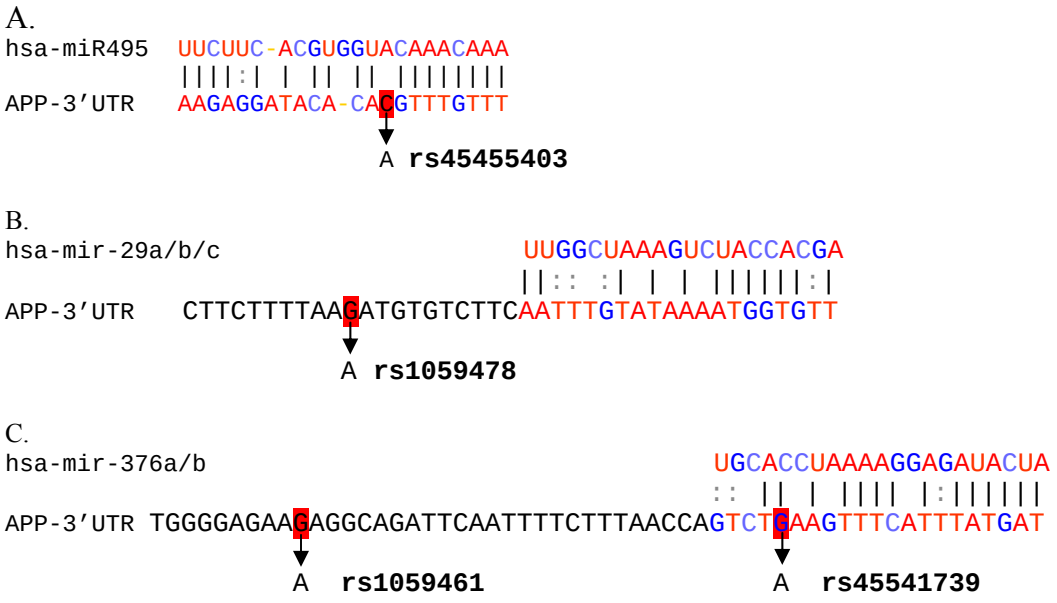

Figure 1: (A) miR-495 target site SNP is located one nucleotide outside of seed region. mir-495 binding to its putative target sequence. Highlighted nucleotide in the SNP with C=major allele and A=minor allele. (B) miR-29a/b/c binding to its putative target sequence with a SNP in *APP* 3'UTR located outside of the miR-29a/b/c target site. Highlighted nucleotide in the SNP with G=major allele and A=minor allele. (C) miR-376a/b binding to its putative target sequence with a SNP in *APP* 3'UTR located outside of the miR-376a/b target site and a SNP within the miR-376a/b target site. Highlighted nucleotide in the SNP with G=major allele and A=minor allele.

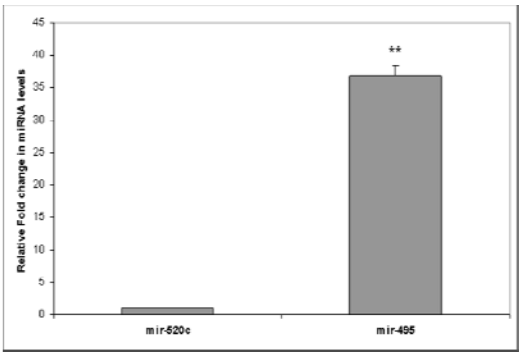

Figure 2: miR-495 expression in normal human brain. miR-495 RNA levels compared to RNU44 RNA levels. miR-520c has been reported to not be expressed in brain.

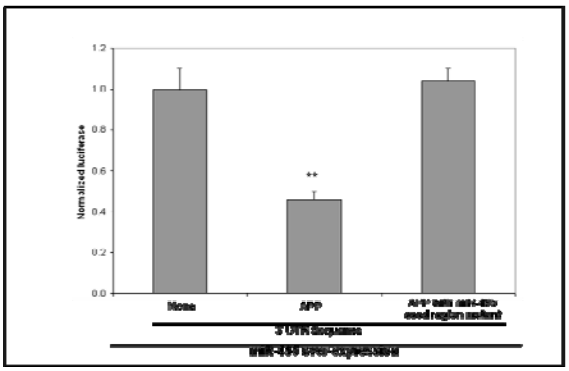

Figure 3: miR-495 over-expression binds to its putative wild-type target sequence, but not the mutated sequence, in APP 3'UTR and regulates reporter gene expression in Naïve 293 cells.

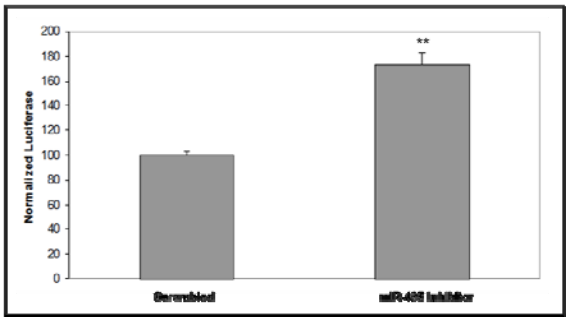

Figure 4: Inhibition of miR-495 increases reporter gene expression.

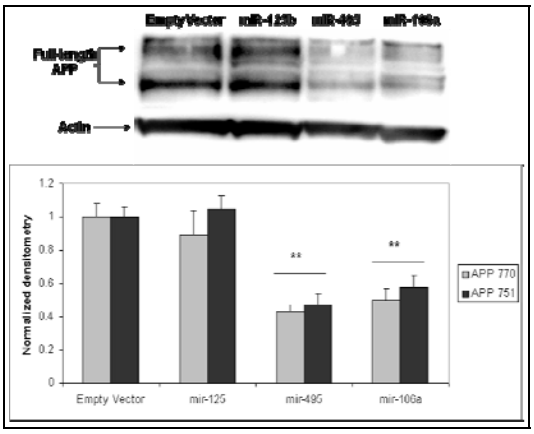

Figure 5: miR-495 over expression significantly decreases endogeneous APP protein levels in Naïve HEK 293 cells. miR-106a is used as a positive control, miR-125b is used as a negative control.

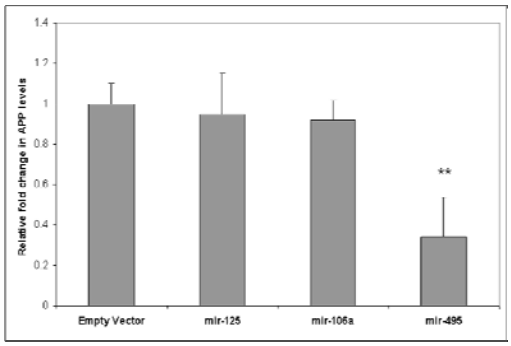

Figure 6: miR-495 over expression significantly decreases APP mRNA levels in Naïve 293 cells. miR-495 over-expression reduces APP mRNA levels unlike miR-106a which has no effect on APP mRNA levels.

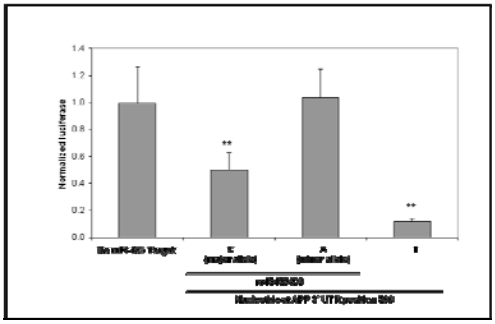

Figure 7: The minor allele of rs45455403 disrupts miR-495 mediated regulation of APP 3'UTR controlled luciferase expression. The APPP 3' UTR was mutated at position 590 from "C" to either "A", the minor allele of rs45455403, or to "T", predicted to be complementary to the corresponding miR-495 base.

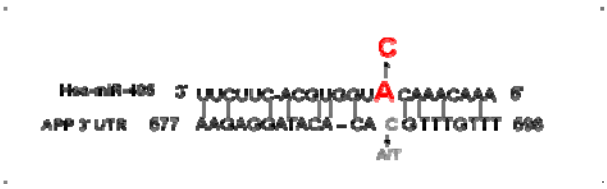

Figure 8: To assess if the allele specific regulation of luciferase activity may also result in allele specific regulation of APP protein levels, we mutated Position 9 of miR-495 since mutating the genomic copy of the *APP* 3'UTR is not possible. Position 9 of the miRNA is predicted to be the miRNA nucleotide corresponding to the rs45545403 allele.

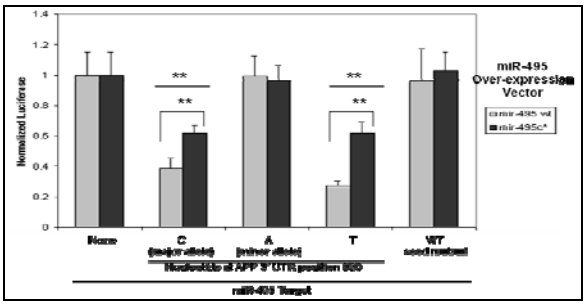

Figure 9: Over-expression of the miR-495 position 9 mutant suppresses miR-495 mediated luciferase expression compared to miR-495 wild type.

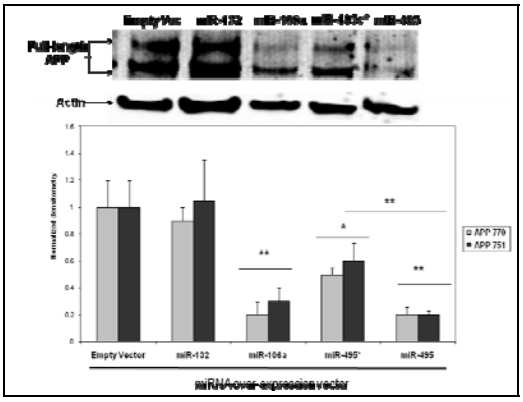

Figure 10: Over-expression of the miR-495 "C" (miR-495*) mutant suppresses miR-495 mediated repression of endogeneous APP levels in Naïve 293 cells compared to miR-495 wild type over-expression.

Research Project 11: Project Title and Purpose

Suppression of Monocyte Migration by Inducible CCR2 Silencing - The purpose of this work is to develop a new method to intervene in the progression of neurologic disease that often occurs in HIV-1 infected individuals. We will investigate a method designed to reduce the ability of

HIV-1 infected immune cells to migrate into the brain. This migration is enhanced by signals released from brain-resident infected cells in a positive feedback loop that we will disrupt using a strategy based on RNA interference. Certain receptors that are present on the surface of immune cells, and that allow these cells to respond to the migratory signals, will be down-regulated specifically in HIV-1 infected cells. If successful, this will lead to therapies designed to reduce the overall inflammatory immune response to infection in the brain and help to curb the progression of neurologic disorders.

Anticipated Duration of Project

1/1/2010 - 12/31/2010

Project Overview

HIV-1 associated dementia (HAD) and a more subtle condition called minor cognitive motor disorder (MCMD) are neurological disorders that develop in a high percentage of HIV-1 patients and correlate with a worse overall outcome. Although control of viral load using anti-retroviral therapies (ART) has reduced the severity of these neurological diseases, longer patient survival times have increased their prevalence. Further, the failure of existing ART to cross the blood brain barrier (BBB) limits its efficacy in treating HIV-1 infection in the brain. In the experiments of this project, we will address these issues by using a lentiviral vector, that we developed in previous work, that expresses a microRNA (miRNA) designed to suppress the expression of a cytokine receptor (CCR2). The vector will be used to tranduce monocytes, where the CCR2 receptor plays a central role in monocyte migration across the BBB in response to MCP-1 (CCL2), a cytokine that is induced by exposure of astrocytes to the viral protein Tat. The CCR2-miRNA is expressed from a Tat-inducible RNA polymerase II promoter and thus silencing is limited to HIV-1 infected cells, protecting the functional integrity of uninfected monocytes. We expect that this strategy will help to interrupt a positive feedback loop where infected monocytes would otherwise be attracted into the brain by MCP-1 that, in turn, was induced by Tat released from brain-resident infected cells. In the current phase of the project, we will test whether transduction with our lentiviral vector affects aspects of monocytes physiology and whether sufficient miCCR2 can be induced by HIV-1 infection to suppress migration of transduced monocytes. We recognize that additional toxic factors are released in the brain of an infected patient and contribute to neuronal damage. The work of this project is meant to be a proof-of-principle study that focuses on a major regulatory circuit, but where additional elements can be added to our highly adaptable silencing vectors in the future.

Principal Investigator

Laura F. Steel, PhD
Assistant Professor
Drexel University College of Medicine
245 N 15th St
MS 1013A
Philadelphia, PA 19102

Other Participating Researchers

Michele A. Kutzler, PhD, Jeffrey M. Jacobson, MD - employed by Drexel University College of Medicine

Expected Research Outcomes and Benefits

This work can provide the basis for a novel approach to HIV-1 therapy that addresses both viral replication and disruptions of cellular signaling that are responsible for much of the pathogenesis of this disease. While there has been a degree of success in the treatment of HIV-1 with current anti-retroviral therapies (ART), these treatments remain problematic in terms of cost, unwanted side effects, patient compliance, and long-term efficacy. In addition, the neurological disorders associated with HIV-1 infection have been particularly difficult to treat since most medications will not cross the blood-brain barrier. The work of this project explores the idea that cellular signaling pathways that affect disease progression can be specifically disrupted in HIV-1 infected cells. By targeting cellular pathways instead of viral gene products, we expect to reduce the problem of escape by this highly mutable virus. However, our strategy also preserves the functionality of important cells of the immune system that are not infected by HIV-1. We expect that this work will help to identify cellular regulatory networks that play key roles in neurological disease progression as well as to develop new strategies to disrupt these networks in a therapeutically significant way.

Summary of Research Completed

The goal of this project is to characterize the efficacy of lentiviral vectors designed to expess microRNAs (miRNAs) that downregulate CCR2 on the surface of human primary monocytic cells. In the first six months of funding, we have concentrated on increasing the potency of silencing from our miCCR2 constructs, establishing an assay system for knockdown of CCR2 on the cell surface, and developing procedures for the isolation and transfection of human monocytic cells.

Knockdown of endogenous CCR2

In the initial construction and testing of CCR2-miRNA expression plasmids, the efficacy of the CCR2-miRNAs was tested against a dual luciferase reporter plasmid where target sequence is inserted into the 3'UTR of a Renilla luciferase (Rluc) gene and activity is measured by reduced expression of Rluc relative to independently expressed firefly luciferase (Fluc). Using this assay, we identified miCCR2-D as a construct with some efficacy against CCR2-mRNA derived targets. While these assays serve as an initial screen for effective CCR2-miRNAs, silencing against endogenous CCR2 mRNA must be confirmed. To do that, we sought to establish that CCR2 is expressed on the surface of U937 cells, a human monocytic cell line, and that expression could be reduced by our CCR2-miRNA. While we were successful in detecting CCR2 expression on the surface of U937 cells by FACS analysis (see Figure 1), the efficiency of transfection of these cells was too low to evaluate CCR2 knockdown by this method.

To address this problem and test our miCCR2 plasmid against CCR2 mRNA, we used 293T cells that are notable for their high efficiency of transfection. These cells do not express endogenous CCR2 and therefore we transfected them with a CCR2 expression plasmid, pCMV-CCR2, together with the silencing plasmids to be tested. 48 hours after transfection, cells were reacted with antibody to CCR2 and analyzed by FACS. Results in Figure 2 show that in 293T cells, surface expression of CCR2 from the transfected plasmid can be suppressed by approximately 15% by miCCR2-D. This is significant, but less than the levels of suppression indicated in our original dual luciferase assay screens of miCCR2 constructs.

Therefore, we have constructed and tested three additional candidate CCR2-miRNAs (constructs E, F, and G). Two of these were derived from the Open Biosystems Library that we used previously, and one was constructed according to a web-based algorithm. All were built into the pUC-based vector described previously where expression of the miRNA is driven by a U6 (RNA polymerase III) promoter. Knockdown of CCR2 mRNA was assayed in HEK-293T cells that were transfected with pCMV-CCR2, together with the silencing plasmids to be tested. RNA was isolated from cells 48 hours post-transfection and reductions in CCR2 mRNA were measured by RT-PCR. In these experiments, we confirmed the activity of miCCR2-D and identified two additional CCR2-miRNAs (constructs E and G) that showed silencing activity (see Figure 3). Since our published work has demonstrated that miRNAs can be expressed from polycistronic constructs that show increased potency compared to the constituent monocistronic constructs, we have now generated the combined miCCR2-D/E construct, a bi-cistronic construct that expresses both miCCR2-D and E, and are proceeding with testing of this new silencing plasmid. If necessary, we will add miCCR2-G, as well.

Isolation of monocytes from human peripheral blood mononuclear cells

Human peripheral blood mononuclear cells (PBMCs) were isolated by sequential centrifugation on Ficoll-Hypaque and Percoll gradients (Amersham Pharmacia LKB, Piscataway, NJ). For isolation of monocytes, $CD14^+$ cells were purified from PBMC by positive enrichment using autoMACS (Miltenyi Biotec, Auburn, CA) according to the manufacturer's instructions. The purity of the monocyte cell populations isolated was >98% as determined by FACS. Results in Figure 4 show that the $CD14^+$ monocytes are expressing CCR2, as indicated by positive staining with a CCR2 antibody.

Methods: For FACS staining, single cell suspensions were washed in PBS (pH 7.2) containing 0.2% bovine serum albumin and 0.1% NaN_3. Cells were incubated with goat IgG to block binding of Ig to FcßR and stained with PercP, FITC, APC or PE-labeled specific mAb diluted to the optimal concentration for immunostaining for 30 min at 4°C, washed three times and analyzed by flow cytometry. Live cells were gated on the basis of their forward scatter and side scatter characteristics and analyzed directly on a BD FACsCaliber Flow Cytometer (Coulter, Hialeah, FL) using FlowJo software (TreeStar, San Carlos, CA). All samples were compared to their isotype-matched controls. In the case of dual flow cytometry individual samples treated with each isotype alone were used to determine the background levels of auto fluorescence.

Antibodies: Conjugated human mAbs to CD14, CD86, HLA class II DR were purchased from BD Biosciences Pharmingen (San Diego, CA).

Generation and culture of human monocyte-derived macrophages

Monocyte derived macrophages (MDM) were generated from monocytes prepared from PBMCs. In brief, adherent monocytes were cultured in complete RPMI 1640 medium with 1000 U/ml of recombinant human (rh) MCSF (Peprotech, Inc.) per 10^6 cells for up to 5 days. MDM were phenotyped using HLA-DR^{+++}, CD86^{+++}, and CD14^{+++}. All cytokines were recombinant human proteins and were used at plateau concentration to induce the optimal generation of MDM. The FACS analysis shown in Figure 5 demonstrates the differentiation of monocytes into macrophages by four days of treatment with MCSF.

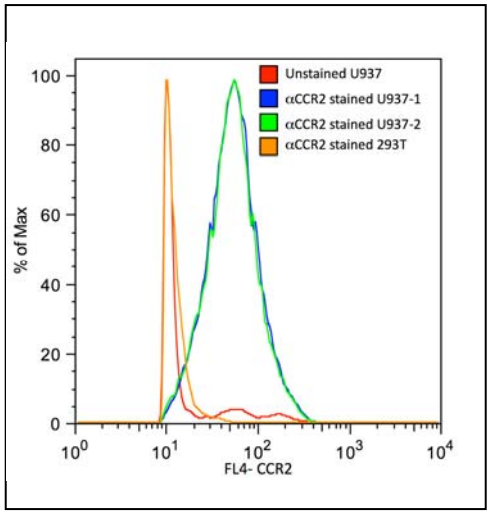

Figure 1. Cells of the monocytic line, U937, express CCR2 on their surface, as detected by FACS analysis. U937 cells or 293T (control) cells were stained with antibody to CCR2 and analyzed by FACS.

Figure 2. FACS analysis of 293T cells shows suppression CCR2 expression by miCCR2-D. 293T cells were co-transfected with pCMV-CCR2 together with no silencing plasmid, pUC-U6-miCCR2D, or pUC-U6-miEGFP, as indicated. 48 h post-transfection, cells were stained with antibody to CCR2 and analyzed by FACS.

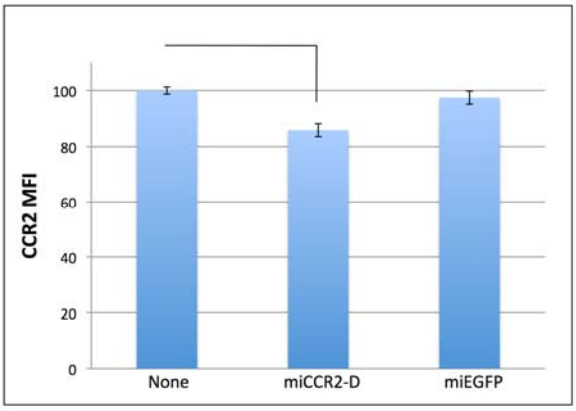

Figure 3. RT-PCR analysis of miCCR2 candidates. HEK-293T cells were transfected with pCMV-CCR2 together with pUC-U6-miCCR2-D, -E, -F, -G, or a non-specific control miRNA. Knockdown of CCR2 mRNA was assessed by RT-PCR. Actin mRNA was detected in each sample as a control. Each construct was assayed in duplicate transfections.

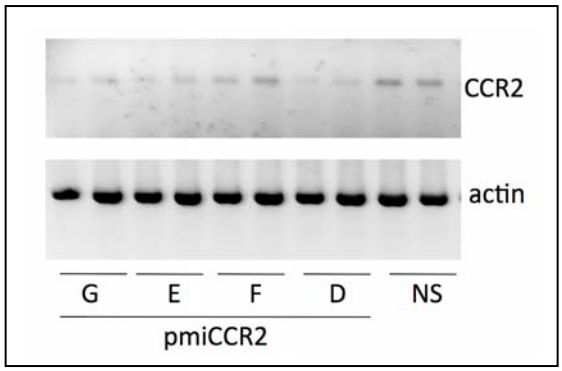

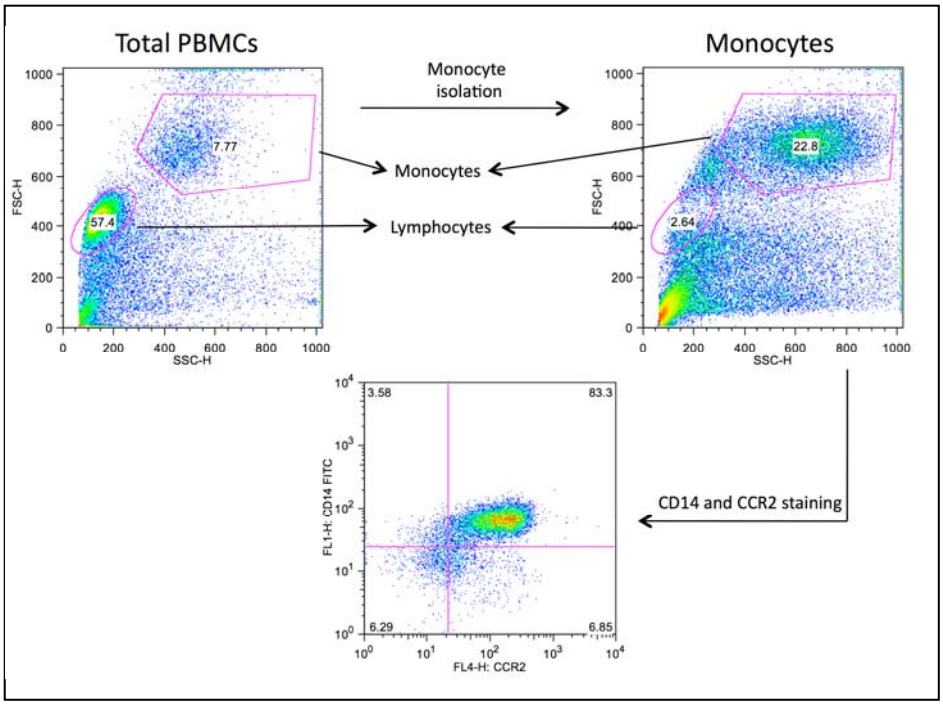

Figure 4. CCR2 is expressed on the surface of isolated human monocytes. The monocytic cell population was isolated from human PBMCs as described in the text. The identity of monocytes was confirmed the marker CD14; CCR2 expression on the monocytes was demonstrated by anti-CCR2 staining.

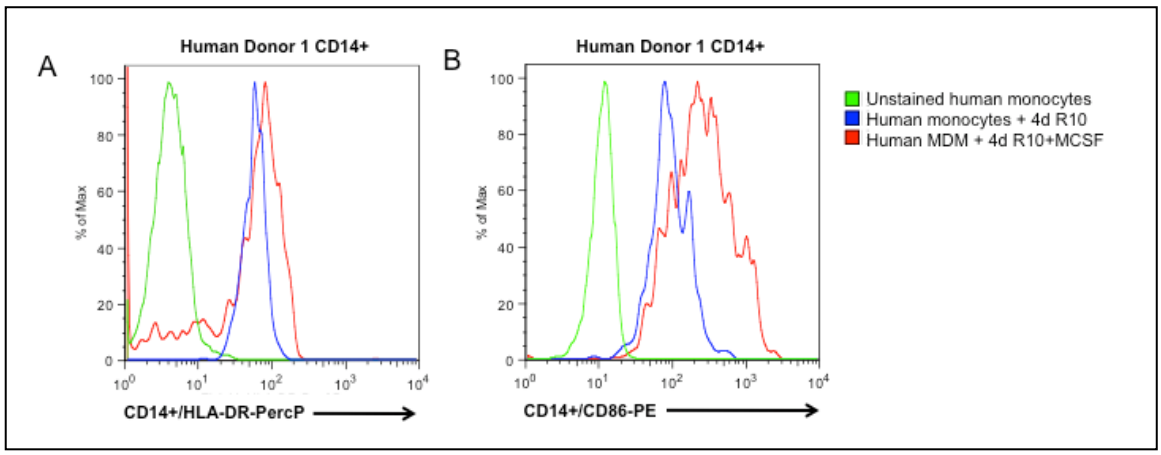

Figure 5. FACS analysis demonstrating differentiation of isolated human monocytes into macrophages (MDM) as determined by HLA-DR+ and CD86+ staining on CD14+ cells following 4 days of treatment with M-CSF.